THz Low Resolution Spectroscopy for Astronomy

Gordon J. Stacey

(Invited Paper)

***Abstract*—The THz spectral regime provides a wide range of spectral lines that are invaluable probes of star formation and AGN activity in galaxies both in the local Universe and at the earliest times. We review the utility of these lines, give examples of the science they deliver, and detail the properties of successful low resolution direct detection spectrometers for work in the THz regime. We finish with a discussion of the exciting new science we expect with the next direct detection generation spectrometers on new facilities such as SOFIA, CCAT, SPICA, and ALMA.**

***Index Terms*—Direct detection receivers, extragalactic spectroscopy, fine-structure lines, TH spectroscopy.**

I. Introduction

THE THz spectrum, here loosely defined as frequencies between 600 GHz and 6 THz, contains a plethora of readily detectable spectral lines that are important diagnostics for both the physical and chemical conditions of the gas and the sources of energy within astrophysical environments. These spectral probes include rotational lines from simple molecules (e.g., HD, CH, OH, CO, NH_3, H_2O), and the ground state fine-structure lines from abundant atoms and ions (e.g., C, C^+, N^+, N^{++}, O, and O^{++}). These lines are well explored in both galactic and extragalactic environments, and indeed the molecular lines can be important probes of planetary atmospheres in the solar system. Important results are obtained with both coherent (heterodyne) and incoherent (direct detection) spectrometers. Here we focus on work done with direct detection spectrometers whose natural niche is the broad spectral line environment of extragalactic studies. In this context, line widths are $\sim$ 50 to 500 km/sec, the smaller values typical for low mass dwarf galaxies and spiral galaxies viewed "face-on" and the larger values more typical for more massive systems with more arbitrary presentations on the sky. This narrows our focus to the lines with large luminosities on galactic scales. These are the lines that are important coolants of the interstellar medium (ISM) including the fine-structure lines of C, C^+, N^+, N^{++}, O, and O^{++}, and the mid-J rotational lines of CO.

This paper is divided into five sections. Following this introduction, Section II discusses these spectral lines and their utility as probes of astrophysical environments, Section III is a brief history of observations of these lines including some exciting new astrophysical discoveries, Section IV is a discussion of the merits of direct detection systems, Section V gives examples of moderate resolving power direct detection systems that are used for astrophysical experiments today, and Section VI discusses some of the prospects for future work.

Manuscript received April 08, 2011; revised June 06, 2011; accepted June 07, 2011. Date of current version August 31, 2011. This work was supported in part by NSF Grants AST-0705256 and AST-0722220.

The author is with the Department of Astronomy, Cornell University, Ithaca, NY 14850 USA (e-mail: gjs12@cornell.edu).

Color versions of one or more of the figures in this paper are available online at http://ieeexplore.ieee.org.

Digital Object Identifier 10.1109/TTHZ.2011.2159649

II. Astrophysical Probes Within the THz Bands

A. Fine-Structure Lines

Atoms or ions with ground state electronic configurations that contain valence electrons will have their configurations ordered by the residual electrostatic interaction into terms that differ in the total (vector) orbital angular momentum ($\mathbf{L} \equiv \sum \boldsymbol{l}_i$) and total (vector) spin angular momentum ($\mathbf{S} \equiv \Sigma \mathbf{s}_i$). These terms are donated by ^{2S+1}P, where the superscript $2S+1$ is equivalent to the number of levels into which the term is split, and P denotes the total orbital angular momentum of the electronic term and follows the usual convention where $S, P, D, F \ldots$ refer to terms of $L = 0, 1, 2, 3 \ldots$. These terms are further split by the spin-orbit interaction into levels $^{2S+1}P_J$ where the subscript J denotes the magnitude of the vector sum of $\mathbf{L}$ and $\mathbf{S}$: $\mathbf{J} \equiv \mathbf{L}+\mathbf{S}$. Each of these levels, J, has a degeneracy given by $g_J = 2J + 1$. When an atom or ion has 1, 2, 4, or 5 equivalent p electrons in its ground state configuration, the ordering and selection rules dictate that its ground state term will be ^3P or ^2P terms, so that it has ground state fine-structure lines. After H and He, which have no significant lines in the THz regime, the three most abundant elements in the Universe are oxygen, carbon, and nitrogen with relative abundances $\sim$ 6, 3, and 1×10^{-4} with respect to hydrogen respectively. Amongst these elements, the O, O^{++}, C, C^+, N^+, and N^{++} ionization states have ground term split into fine-structure levels that emit photons in the THz range (Table I). Since transitions within a term involve no change in the electronic configuration, they are forbidden to electronic dipole radiation and decay by magnetic dipole transitions. As such, the excited fine-structure levels are metastable with lifetimes measured in days.

Since they lie in the THz range, where the corresponding wavelengths ($\sim$ 100 μm) are large compared to the typical sizes of interstellar dust grains ($\sim$ 0.1 μm), these lines are largely unaffected by the interstellar extinction by grains that hinders optical and near infrared observations. With weak Einstein A coefficients, the lines are also not usually affected by self-absorption (they are *optically thin*) so that typical photons will escape an emitting gas cloud. Furthermore, the energy levels that emit the lines lie within a few hundred K of the ground state, so that they are easily collisionally excited by electrons, H, or H_2 impacts in many astrophysical environments. The combination makes these THz lines important coolants for many phases of

TABLE I
SELECTED THz SPECTRAL LINES.

Species	Trans.	E.P.[1]	λ (μm)	ν (GHz)	A (s^{-1})	n_{crit} (cm^{-3})[2]
O^o	$^3P_1$ - $^3P_2$	228	63.18	4745	9.0×10^{-5}	4.7×10^5
	$^3P_0$ - $^3P_1$	329	145.53	2060	1.7×10^{-5}	9.4×10^4
O^{++}	$^3P_2$ - $^3P_1$	440	51.82	5786	9.8×10^{-5}	$3.6\times10^{3(*)}$
	$^3P_1$ - $^3P_0$	163	88.36	3393	2.6×10^{-5}	$510^{(*)}$
C^+	$^2P_{3/2}$-$^2P_{1/2}$	91	157.74	1901	2.1×10^{-6}	2.8×10^3 $50^{(*)}$
N^+	$^3P_2$ - $^3P_1$	188	121.90	2459	7.5×10^{-6}	$310^{(*)}$
	$^3P_1$ - $^3P_0$	70	205.18	1461	2.1×10^{-6}	$48^{(*)}$
N^{++}	$^2P_{3/2}$-$^2P_{1/2}$	251	57.32	5230	4.8×10^{-5}	$2.1\times10^{3(*)}$
C^o	$^3P_2$ - $^3P_1$	63	370.42	809.3	2.7×10^{-7}	1.2×10^3
	$^3P_1$ - $^3P_0$	24	609.14	492.2	7.9×10^{-8}	4.7×10^2
^{12}CO	J =13-12	503	200.23	1497	2.2×10^{-4}	2.5×10^6
	J =11-10	365	236.60	1267	1.3×10^{-4}	1.4×10^6
	J = 9 - 8	249	289.12	1037	7.3×10^{-5}	8.4×10^5
	J = 7 - 6	155	371.65	806.7	3.4×10^{-5}	3.9×10^5
	J = 6 - 5	116	433.56	691.5	2.1×10^{-5}	2.6×10^5
^{13}CO	J =12-11	413	226.89	1321	1.5×10^{-4}	1.6×10^6
	J = 8 - 7	190	340.17	881.3	4.5×10^{-5}	1.7×10^5
	J = 6 - 5	111	453.48	661.1	1.9×10^{-5}	2.3×10^5

[1]Excitation potential, energy (K) of upper level above ground. [2]The critical density, n_{crit} is the density at which the rate of collisional depopulation of a quantum level equals the spontaneous radiative decay rate. For species occurring in neutral gas clouds, the collision partners are H and H_2 (assumed T_{gas} = 100 K). For species occurring in ionized gas regions (marked with a (*)), the collision partner is electrons.

the ISM and excellent probes of the physical conditions of the gas clouds and tracers of the sources of heat, be it the radiation fields from nearby stars or AGN, cosmic rays, X-rays or interstellar shocks.

B. Ionized Gas Lines

Ionizing hydrogen requires photons with energy greater than 13.6 eV, so species that require more than 13.6 eV photons to form will be found exclusively within HII regions[1] (O^{++}, N^+, N^{++}), and those with ionization potentials less than 13.6 eV (O, C) will be found exclusively in neutral (hydrogen) gas clouds. C^+ takes only 11.3 eV photons to form, but 24.4 eV to further ionize so that it is found both in neutral and ionized gas clouds. Fine-structure lines are excellent probes of gas density. Fig. 1 shows this sensitivity for the [NII] line pair.[2] Within a species, two fine-structure lines will have different A coefficients, hence different critical densities (n_{crit}) for thermalization of the emitting levels. In the low density limit ($n \ll n_{crit}$), every collisional excitation leads to the emission of a photon, so that the line ratio is constant. In the high density limit ($n \gg n_{crit}$), the levels populations are thermalized, and given by the Boltzman formula therefore yielding a second constant line ratio. Between the low and high density limits the ratios vary strongly with gas density as first one, and then the other emitting level is thermalized. For the lines that arise in ionized gas regions, the level excitation potentials (energy above ground state) are much less than the ionized gas temperatures (~ 8000 K), so that level excitation is very insensitive to gas temperature. However, neutral oxygen and carbon are found in neutral gas regions where gas temperatures are typically between 50 and 1000 K. Therefore, their line ratios *are* sensitive to gas temperature. The critical density of the neutral carbon lines are relatively modest so that the levels are typically thermalized at the densities found in interstellar gas clouds. As such, the [CI] line ratio has proven to be a good temperature probe, and the lines trace gas column density, hence mass.

The THz frequency fine-structure lines are also excellent probes of the hardness of the ambient interstellar radiation fields. The vast majority ($\sim 90\%$) of stars in galaxies like the Milky Way are on the main sequence (MS) where they are fusing hydrogen into helium in their cores. Within the main sequence, stellar luminosities, L_{MS} are strongly dependent on stellar mass, $M : L_{MS} \sim M^{33.5}$. Due to the steep dependence of L on M, the most massive stars are not only the most luminous MS stars, they also have the shortest MS lifetimes, $\tau_{MS} \sim M^{-2.5}$. Furthermore, the most massive MS stars have the highest surface temperatures, T_{eff}, so that they dominate the interstellar UV radiation fields. Therefore, presuming a stellar photospheric origin, a harder ambient UV radiation field indicates more massive stars on the main sequence, hence a younger stellar population. The fine-structure lines trace the radiation field hardness, hence the *age of the stars*. It takes 14.5 eV photons to form N^+ (equivalent $T_{eff} \sim 33{,}000$ K, or a B0 star), and 29.6 eV photons to form N^{++} ($T_{eff} \sim 39{,}000$ K or an O8 star). Therefore, the [NII]/[NIII] line ratios are strongly indicative of the hardness of the ambient interstellar radiation field (Fig. 2). With an ionization potential of 35 eV, O^{++} takes even harder UV photons to form than N^{++}. Therefore, the [OIII]/[NII] line ratios are even stronger indicators of T_{eff}. The [OIII] 88/[NII] 122 μm line is especially useful since the levels that emit these lines have similar critical densities (Table I), so that the resulting line ratio is very insensitive to density as well (Fig. 3).

C. Neutral Gas Lines

In astrophysical environments, as one moves away from the source of ionizing photons there is a transition from regions where hydrogen is fully ionized (the HII region) to the neutral gas clouds beyond. While HII regions and neutral gas clouds have size-scales of the order 10 parsecs (3.1×10^{19} cm), the transition between the two is fairly abrupt. It is roughly given by the mean free path of a photon that is capable of ionizing H, or ~ 0.01 pc for typical interstellar gas densities. Photons with energies less than 13.6 eV escape the HII region and penetrate the neutral gas clouds beyond where they can ionize elements with ionization potentials less than 13.6 eV (e.g., C), and photodissociate molecules with dissociation energies less than 13.6 eV (e.g., CO, H_2, H_2O) forming a photodissociation region (PDR) (see [5]). The full depth of the PDR is often defined as the distance into the cloud to which the cloud physics and chemistry is dominated by FUV ($6 < h\nu < 13.6$ eV) photons. With this definition the PDR can extend to visual extinctions, $A_V > 10$. Most of the far-IR fine structure line radiation arises from the warmer regions closer to the surface within the "C^+" zone, given by the

[1]An HII region is an interstellar gas cloud in which the hydrogen gas is fully ionized.

[2]In astronomical parlance, ionization states of a species, for example nitrogen, are denoted by $N^0, N^+, N^{++}\ldots$ for the neutral, singly ionized, and doubly ionized states etc., while spectroscopic lines are denoted by NI, NII, NIII,… for lines arising from the neutral, singly ionized, and doubly ionized states etc… Brackets around a transition, e.g., [NII] indicate the transition is forbidden to dipole radiation.

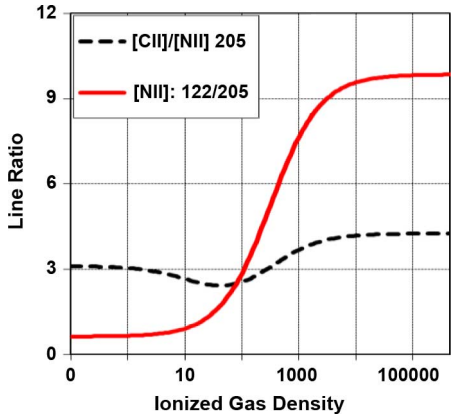

Fig. 1. [NII] 122 μm to 205 μm line intensity ratio as a function of gas density (solid line). This ratio is a sensitive probe of gas density for HII regions with electron densities between 20 and 2000 cm^{-3}. Also shown is the [CII] 158 μm/[NII]205 μm line ratio as a function of gas density. This line ratio is used to discern the fraction of the observed [CII] line that arises from HII regions [2]. This plot assumes a gas phase abundance ratio $n(C)/n(N) = 1.8$ [1], and this ratio is corrected for ionization effects, see [2].

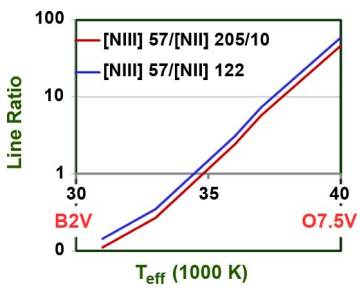

Fig. 2. Ratio of the [NIII] 57 μm to [NII] 122 μm and 205 μm lines as a function of effective temperature of the ionizing star (assumed gas density 1000 cm^{-3}). This line ratio is a very strong diagnostic of the most massive star on the main sequence with line ratios that grow by factors of 1000 when the stellar type changes from B2 to O7.5 stars (based on [3]).

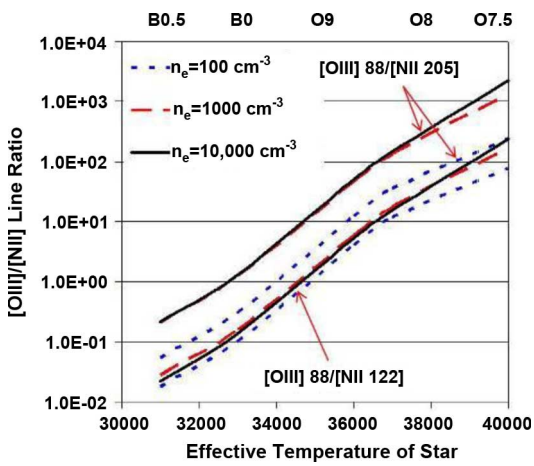

Fig. 3. Ratio of the [OIII] 88 μm to [NII] 122 μm and 205 μm lines for three ionized gas densities as a function of $T_{\rm eff}$ of the ionizing star. This ratio is extremely sensitive to $T_{\rm eff}$ and very insensitive to gas density, especially the [OIII] 88 to/[NII] 122 μm ratio [4] (based on [3]).

depth to which carbon ionizing photons can penetrate forming C^+. This depth is typically determined by the extinction of these photons by dust, and is roughly given by a visual extinction, $A_V \sim 3-4$, which corresponds to a hydrogen column density of $6-8 \times 10^{21}$ cm^{-2}, or ~ 1 pc for a typical gas density of 2000 cm^{-3}. Within the PDR, gas is heated by the photo-electric (PE) effect—whereby hot electrons are ejected from grains by FUV photons and transfer their excess kinetic energy to the gas before recombining with grains. The efficiency of this heating mechanism depends on the grain charge. As the charge on the grain increases, more of the next photon's energy is expended in freeing the electron from the positive potential of the grain, leaving less excess kinetic energy for heating the gas, thereby lowering gas heating efficiency. Therefore, the gas heating efficiency goes down as the ambient radiation field strength goes up. However, this can be mitigated by larger gas densities that will increase electron-grain recombination rates, lowering the grain charge. The PE heating efficiency is typically 0.1 to 1%. The rest of the FUV energy goes into heating the grains which then emit in the THz and infrared continuum. Within the C^+ zone, the gas is primarily cooled through collisional excitation of the ground state fine-structure levels of C^+ and O and subsequent emission in their THz lines. To a lesser extent, the neutral carbon fine-structure lines and the mid-J CO rotational lines are also important coolants for these regions becoming more important at greater depths onto the cloud.

The combination of the [CII] (158 μm), and [OI] (63 and 146 μm) fine-structure lines enables unique determination of PDR gas temperature and density. Since the combined luminosity of these lines gives the gas heating, and the luminosity of the THz dust continuum radiation is directly proportional to the luminosity of the ambient radiation fields, the ratio of the two yields the PE heating efficiency, hence strength of the ambient FUV radiation fields. It can be shown (see [6]–[9]) that for most astrophysical environments that apply over kilo-parsec (kpc) scales in galaxies, the [CII]/far-IR continuum ratio in of itself is an excellent indicator of the FUV field strength and can be used as an indicator of the physical size of the astrophysical source.

A challenge with the [CII] line is that it arises from both ionized and neutral gas regions, so that its diagnostic potential can be problematic. Fortunately, the [NII] 205 μm line has the same critical density for excitation by electron impacts as [CII] so that the [CII]/[NII] 205 μm line ratio from HII regions is only a function of the assumed N^+/C^+ abundances within the HII region (see Fig. 1). Therefore, the [NII] 205 μm line strength yields the fraction of the observed [CII] emission that arises from ionized gas ([2]), and the [CII]/[NII] combination constrains the physical conditions of two major components (ionized and PDR) of the ISM.

D. The Importance of the THz Fine-structure Lines

The THz fine-structure lines are bright. For star forming galaxies, the brightest of these lines is typically the 158 μm [CII] line which can be the brightest single spectral line from the galaxy as a whole, and typically accounts for between 0.1 and 1% of far-IR luminosity of the system ([7]). From the Milky Way galaxy this amounts to 70 million solar luminosities ($L_\odot$) [10], [11], for nearby ultraluminous infrared galaxies, those with far-IR luminosities exceeding 10^{12} $L_\odot$ the [CII] line can have luminosities of $10^9 L_\odot$ ([12]), while in distant hyper-luminous galaxies ($L_{\rm far-IR} > 10^{13} L_\odot$), ten billion solar

luminosities of power often emerges in this single line ([9], [13])! Other lines, in particular [OI] 63 μm and the [OIII] lines often are nearly equal in luminosity to the [CII] line and the [NIII], [NII], and [OI] 146 μm lines are only a factor of 5 to 10 fainter [14]. The [OI] and [CII] lines are especially bright because they are the cooling lines for a dominant component of the ISM, PDRs. Cooling lines are important as an interstellar cloud must cool to enable it to collapse to form the next generation of stars. It is the extinction-free nature, and powerful diagnostic utility of these lines, together with their intrinsic brightness that makes their study so compelling, even from the most distant sources in the Universe.

E. Molecular Lines

The brightest of the molecular lines in the THz regime are the mid-J rotational lines of CO. These lines probe the warm, dense gas immediately interior to the atomic regions in PDRs and can be quite strong in molecular shocks. The run of line intensity with J constrains the physical conditions of the emitting gas. Several of the rotational lines can be optically thick, so that radiative transfer effects must be considered. Typically radiative transfer is handled within a "large-velocity gradient" model. These models have degeneracies between optical depth effects, and those of gas excitation (density and temperature), so that it is important to measure low optical depth isotopologues of CO, most commonly ^{13}CO transitions to break these degeneracies. The absolute strength of the lines compared to the THz continuum and fine-structure lines can reveal the source of heat. For example, strong CO lines and relatively weak THz lines indicates non-PDR origins for the CO emission: the gas may be heated by super-sonic shocks, cosmic rays or X-rays [15]–[18].

F. The Importance of the THz Molecular Lines

Stars form from dense molecular clouds. To enable sustained collapse, clouds must cool through THz line radiation. Studies have shown that up to half of the molecular ISM in starburst[3] galaxies is warm and dense [15], [16], [18]–[20] so that it is important to study this gas through its mid-CO cooling line emission to understand the interplay between star formation and the natal molecular clouds. For example, for some starburst nuclei, supernovae blasts might compress the ISM leading to the formation of the next generation of stars so that the starburst is self-sustaining, while for others far-UV and cosmic ray heating, and molecular flows may energize or disrupt the ISM making the starburst self-limiting [16]. Notice that since the low J ($J < 4$) lines have smaller excitation requirements, their line ratios are relatively insensitive to the physical parameters of the warm dense gas.

III. Astrophysical Observations

A. A Short History

The far-IR fine-structure lines discussed above were recognized as important astrophysical coolants long before their detection, cf. [21]–[23], but their astrophysical detection was hindered by (1) the strong telluric absorption from water vapor which makes detection of all but the [CI] lines nearly impossible from ground based telescopes, (2) the uncertain transition frequencies of the major lines, and (3) the still emerging state of detector technology at this time. The primary issue was telluric absorption, which was largely erased with the advent of airborne and balloon borne telescopes in the 1970's. At altitudes above 12.5 km, one is typically above 99.8% of the atmospheric water vapor, opening up the THz windows, so that the THz lines were soon detected from these facilities. The [OIII], [OI], and [CII] lines were first detected by Martin Harwit's group at Cornell University using a grating spectrometer on the 30 cm telescope in NASA's Lear Jet Observatory [24]–[28]. The [NIII] line was first detected by the ESA/ESTEC and University College, London (UCL) groups using their Michelson Fourier transform interferometer (FTS) on their balloon-borne 60 cm telescope [29], [30]. The [NII] lines were first detected with the FIRAS FTS on the COBE satellite [11] at about the same time they were also detected by Edwin Erickson's group at NASA Ames using a grating spectrometer on the 91 cm telescope on NASA's Kuiper Airborne Observatory (KAO) [31]. Tom Phillips group at Caltech made the first detection of the [CI] 492 GHz line with a heterodyne receiver on the KAO [32], while the Betz/Genzel group at UC Berkeley obtained the first detection of the 809 GHz [CI] line by using a heterodyne receiver on the UH 88" telescope [33]. Several of these lines were also mapped with balloon-borne experiments including the mapping of the inner Galaxy in [CII] by Okuda's group at ISAS in Japan using their Fabry–Perot interferometer (FPI) [34], and mapping of the Orion Nebula in several lines with the ESA/UCL Michelson interferometer [35]. These galactic observations were soon followed up by extragalactic FPI work in the Townes/Genzel group at UC Berkeley and at MPE Garching (e.g., [7], [36]–[38]) and within Edwin Erickson's group at NASA Ames ([39]–[41]). All of these observations of lines with wavelengths shorter than 210 μm were obtained with direct detection spectrometers (gratings, FTS, and FPI).

The first THz molecular lines detected from external galaxies were the bright mid-J CO rotational lines. These lines were first detected using heterodyne receivers from galactic sources. The first mid-J CO line detected from an extra-galactic source was the CO(6–5) line at 690 GHz, detected from the nearby starburst nuclei of NGC 253, M82, and IC 342 using a Schottky-diode based receiver [19]. The CO(7–6) (809 GHz) line was first detected and mapped from an extragalactic source in the local Universe, NGC 253 using a direct detection spectrometer, SPIFI ([15] see below). (The line had previously been detected from high redshift sources, e.g., [42]). The first extra-galactic mid-J line of ^{13}CO detected was the 6–5 line, also detected from NGC 253, using the ZEUS grating spectrometer, ([16] see below).

In 1996, ESA launched the Infrared Space Observatory, a 60 cm cooled telescope in Earth orbit that contained both a FPI and a grating spectrometer for THz spectroscopy. The space-based platform opened an un-obscured view of these lines, albeit at wavelengths shorter than the long wavelength cut-off of stressed Ge:Ga photoconductors, near 200 μm. An example of ISO based fine-structure line science is outlined below. ISO

[3]A starburst galaxy is one that is forming stars at such a high rate that it will exhaust is supply of star forming gas in a timescale short compared to the lifetime of the Universe.

also for the first time detected several molecules in absorption against the THz continuum from an extragalactic source [43], [44]. (OH and CH, and ^{18}OH had previously been reported in absorption against the THz continuum of Sgr B2 [45]–[47]). The THz spectrum of the heavily imbedded nucleus of Arp 220 in particular shows many absorption lines (e.g., OH, H_2O, CH, NH, NH_3) which are excellent tracers of very small gas column densities, and gas phase molecular abundances [43]. As these rotational lines are permitted transitions, they are well coupled to the local radiation fields and have been used to constrain source geometry and the properties of the sources of the THz continuum radiation [44].

B. M82: A Case Study

There have been many excellent studies of nearby galaxies in the THz fine-structure lines since the discovery observations outlined above. For brevity, we focus on studies of M82, the brightest extragalactic THz source in the sky, and the nearest starburst galaxy. In normal star forming galaxies like the Milky Way about 17% the ISM is in molecular clouds with size-scales of 20 to 40 pc, 60% is in PDRs, and 23% is in diffuse HII regions [48]. The PDR mass is dominated by the relatively diffuse atomic ISM, but a significant fraction ($\sim 20\%$) of the PDR mass is contained in dense PDRs formed on the FUV exposed surfaces of molecular clouds. In contrast, KAO studies of M82 that included the [OI], [OIII], [NII], [NIII], and [CII] lines revealed an ISM fragmented by the powerful starburst into tiny ~ 1 pc diameter molecular cloudlets [41]. These cloudlets are substantially warmer and denser than Milky Way counterparts, and only half the mass of these cloudlets is molecular. The rest—nearly half the total ISM—is contained within dense PDRs on these molecular cloudlet surfaces. This large mass fraction in dense PDRs is due to the intense FUV radiation field from the starburst. This radiation field is about 1000 times stronger than that of the solar neighborhood and extends over a 300 pc scale region in the center of M82. The high pressure clouds are in near pressure equilibrium with ionized gas and a hot inter-cloud medium that is 10–20% of the total interstellar gas mass. Subsequent studies based on ISO LWS spectroscopy (cf. Fig. 4) of these lines strongly constrained the stellar mass function. It is best modeled as a 3 to 5 million year old instantaneous starburst with a 100 solar mass upper limit to the initial mass function [49].

C. Recent Results: Herschel and Markarian 231

ESA launched the 3.5 m aperture passively-cooled Herschel Space Observatory (HSO) on May 14, 2009. It is expected to operate until its cryogen supply runs out sometime in early 2013. Herschel is dedicated to far-IR and submm wavelength photometry and spectroscopy and is performing at or beyond expectations in nearly every mode. Of relevance to the discussion here are the Photodetector Array Camera and Spectrometer (PACS) and the Spectral and Photometric Imaging Receiver (SPIRE) spectrometers operating in the 55 to 210 and 194 to 671 μm spectral regions respectively (see Section V). These direct detection spectrometers have been enormously successful delivering a wide variety of science from studies of the planets to star

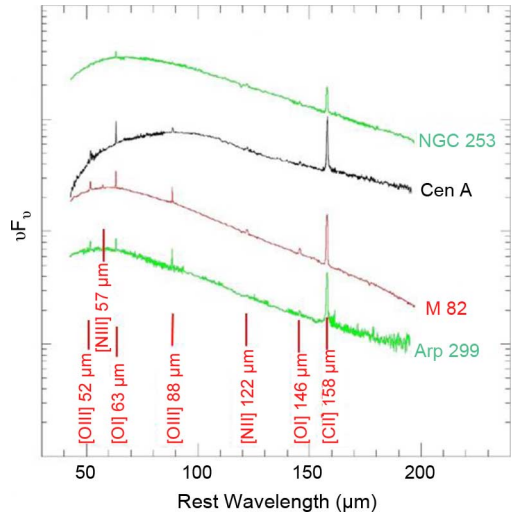

Fig. 4. ISO-LWS spectra of four infrared bright galaxies fromm 44 μm to 196 μm showing most of the bright THz fine-structure line. Adapted from [50].

formation in galaxies at redshifts beyond 2.2—when the Universe was less than 3 Giga years old. In this section, we briefly describe the SPIRE results obtained on Mrk 231.

Mrk 231 is a representative of the Ultraluminous Infrared Galaxy (ULIRG) class of galaxies that were originally discovered by the IRAS satellite. These galaxies emit most (up to 99%!) of their bolometric luminosity in the THz dust continuum and by definition have THz dust continuum luminosities in excess of $10^{12}L_\odot$. The large THz to optical luminosity ratio means their source(s) of radiant energy, be it stellar photospheres or accretion disks enveloping super-massive black holes, are enshrouded in many magnitudes of extinction by dust. The obscuring dust absorbs the optical radiation, heats up, and re-radiates the energy in the THz continuum. Most ($\sim 70\%$) of the ULIRGs are thought to be powered primarily by star formation, with the rest powered primary by AGN [51]. Mrk 231 is from the "mixed" class, so it will show characteristics of both. Fig. 5 shows the remarkably rich SPIRE FTS spectrum of Mrk 231 [52]. Within this spectrum are 25 detected lines including lines of CO from $J = 5 - 4$ up to $J = 13 - 12$, 7 lines of H_2O [53], 3 of OH^+, and one each of H_2O^+, CH^+, and HF. The CO rotational spectrum up to $J = 8 - 7$ is consistent with line emission from warm, dense PDRs enveloping intense regions of star formation. At higher J, the spectrum flattens out with near uniform intensity. This flattening of intensity at the highest J is predicted for an X-ray dominated region (XDR)—a molecular region whose primary source of heat is intense X-ray illumination [54]. The XDR is very likely associated with the "confining torus" of molecular gas thought to envelope the AGN, and the source of X-ray radiation is most likely the AGN itself. The strong OH^+ and H_2O^+ line emission strongly support the XDR heating mechanism. This is the first direct detection of the hot molecular torus long thought to circulate about the supermassive black holes that power AGN.

D. Recent Results: The Early Universe

The COBE satellite discovered that integrated over the history of the universe, half of the photospheric emission from stars

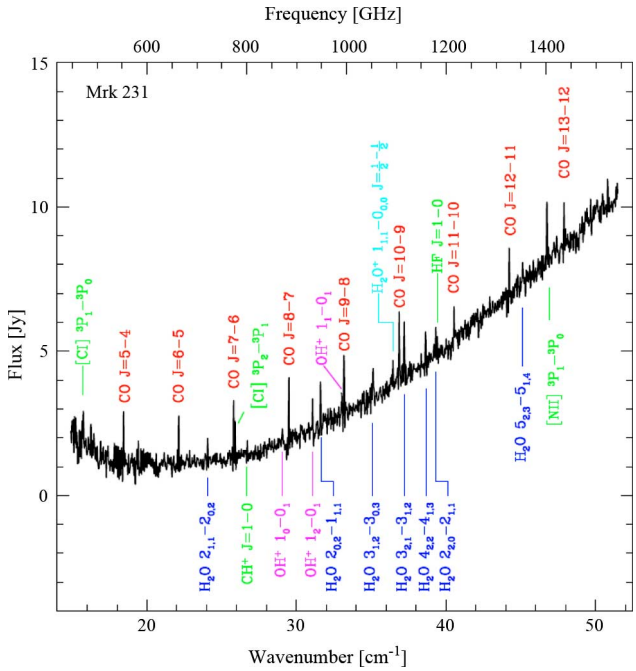

Fig. 5. SPIRE FTS spectrum of the ultraluminous galaxy Mrk 231 [52]. Red, blue, magenta, and cyan lines are CO, H_2O, OH^+, and H_2O^+, respectively.

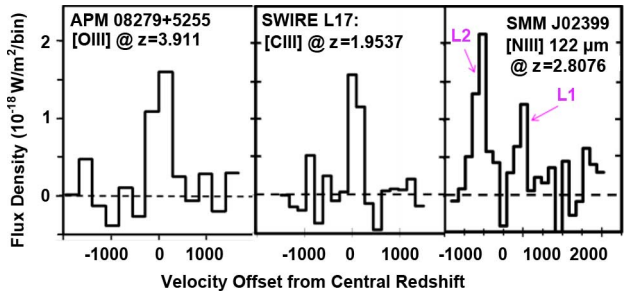

Fig. 6. ZEUS/CSO detections of [OIII] 88 μm, [CII] 158 μm, and [NII] 122 μm fine-structure lines from high redshift systems [63], [9], [4].

is absorbed by dust in their nascent molecular clouds [55], [56]. The heated dust then reradiates its energy in the FIR, with power typically peaking in a broad band centered near $60-100$ μm. Much of this cosmic infrared background was subsequently resolved by large and sensitive telescopes into several classes of luminous star forming galaxies that emit primarily in the FIR to submm bands (~ 30 μm $< \lambda <$ 1 mm), most of which lie at redshifts beyond 1 or look-back times beyond 7.7 Giga years (Gyr) [57], and indeed, the peak of star formation activity per unit co-moving volume occurred between redshifts 1 and 3 (2 to 6 Gyr after the Big Bang) at a rate 10–20 times the current value [58]. Continuum surveys are the means of discovery for these distant galaxies, but spectroscopy is the only method for unraveling the physics of the interstellar medium and the properties of the stellar populations. Since these systems are highly obscured, FIR/submm spectroscopy is key to these studies.

The [CI] lines were the first THz fine-structure lines detected at high redshift, detected from the lensed Cloverleaf quasar at $z = 2.56$ [42], [59]. These lines, together with CO lines, were used to show that the molecular disk has surprisingly modest mass within this system. The brightest THz fine-structure line, the [CII] line was first observed at high redshift from the very high redshift ($z = 6.42$) quasar, SDSS J1148 + 5251 [60]. The line was subsequently detected in two other high z ($z > 4.4$) quasar dominated systems, each of which show a low $L_{[CII]}/L_{FIR}$ ratio reminiscent of that found in some ULIRG galaxies in the local Universe [61], [62]. In local ULIRGs this low ratio is interpreted as either intense FUV fields lowering the $L_{[CII]}/L_{FIR}$ luminosity ratio since [CII] line saturates, while continuum does not, or due to presence of additional non-PDR origin for the FIR continuum [12].

The first detection of a high z [CII] line from the $z = 1-3$ epoch of peak star formation in the Universe, and also the first detection of [CII] from a high z galaxy not association with a quasar was made from MIPS J1428 at $z = 1.33$ using the ZEUS spectrometer [8]. Here the $L_{[CII]}/L_{FIR}$ ratio is large, comparable to nearby starburst galaxies, and when combined with the CO(1–0) line, indicates the ISM in MIPS J1428 contains molecular clouds with similar gas densities and exposed to similar radiation fields as those found in M82. But, since MIPS J1428 is forming stars at the rate of 1800/year compared to ~ 5/year for M82, the starburst must be enormous in this source, with an estimated diameter of 3–8 kpc, essentially involving the entire galaxy. This first detection was followed up by a [CII] survey containing 12 detections of galaxies in the $z \sim 1$ to 2 interval in the [CII] line quadrupling the numbers of high z systems then reported [9] (Fig. 6). Within this survey, those systems that derive most of their energy from star formation have a $L_{[CII]}/L_{FIR}$ luminosity ratio eight times that of those that derive most of their energy from AGN activity, so this ratio picks out systems dominated by star formation. As for MIPS J1428, the star formation dominated systems have starbursts similar in intensity to that of M82, but the starbursts extend over kiloparsec scales—very unlike the confined (few hundred pc scales) found for starbursts in local starburst or ULIRG galaxies. Essentially the entire galaxy is erupting in a super-massive starburst. Clearly the mode of star formation is quite different at early times than it is today.

The THz fine-structure lines of [OIII] are now reported from high z systems. The 88 μm line was detected first from two AGN/starburst systems at high redshifts using the ZEUS spectrometer on the CSO [63] (Fig. 6). For SMM J02399 ($z = 2.8$), the line was used together with the THz continuum to estimate the age of the starburst and most massive star on the main sequence. For APM 08279 ($z = 3.9$) it was found that the line could arise from either the narrow line region of the AGN, or from a starburst headed by O7.5 stars. Very recently, the [NII] 122 μm line was detected for the first time at high z, from SMM J02399 and the Cloverleaf [4] (Fig. 6). The [OIII]/[NII] line ratio tightly constrains the radiation field (Fig. 3), and it is found that SMM J02399's current stellar population is dominated by O9.5 stars, indicating a 3 million year old starburst.

The [OIII] 52 μm line was detected by PACS on the HSO from MIPS J1428 ($z = 1.3$), and IRAS F10214 ($z = 2.28$) [64]. The line is compared with the THz continuum to show that the former source is similar to local starburst galaxies, while the latter is similar to local ULIRGs. The first high z detection of [OI] 63 μm (from MIPS J1428) was also reported in this paper, confirming the [CII] based conclusions [8].

IV. Direct Detection Spectroscopy

It is very challenging to achieve very high spectral resolving powers (RP) with direct detection systems in the THz regime. For instance, in a single pass configuration, a grating spectrometer with $\mathrm{RP} \equiv \nu/\Delta\nu \sim 10^5$ at 1 THz ($\lambda = 300$ μm) needs an effective delay path, $d \sim 10^5 \cdot 300$ $\mu\mathrm{m}/2 = 15$ meters. Even within a multiple pass system, like a Fabry–Perot with finesse ~ 30 the path is still a challenging 50 cm. Therefore, the only reasonable way to achieve these very high RP at THz frequencies is with heterodyne detection techniques. However, for the modest RP required for extragalactic spectroscopy (1000), delay paths are modest (~ 15 cm) so that direct detection spectrometers are straightforward to construct.

In an incoherent, or direct detection spectrometer the energy of the incoming photon is used to create a signal either by heating a detector (as in a bolometer) or in causing an electron to make a quantum transition from a valence to conduction band in a semi-conductor (as in a photoconductor). A coherent, or indirect detection system relies on the wave nature of light. The advantage of a coherent receiver is that the spectral RP can be made extremely high, and the preservation of phase makes them easy to use for aperture synthesis. The systems we compare to in the THz band are heterodyne receivers, where the THz wave from the astronomical source is beat against a local oscillator to mix the signal down to gigahertz frequencies where it is efficiently detected in a square law mixer—one who's output signal power is proportional to the square of the input field strength—such as an SIS mixer. Coherent detection preserves photon phase and requires signal amplification before detection. This results in an uncertainty in photon occupation number of one photon/Hz/sec. This "quantum noise" when expressed in terms of temperature of a radiation field that produces the same noise, is given by $\mathrm{T_{QN}} = \mathrm{h}\nu/\mathrm{k} = 48(\nu/\mathrm{THz})\mathrm{K}$, where h and k are Planck's and Boltzman's constants respectively. The quantum noise is unavoidable, and imposes a sensitivity floor for the receiver noise temperature of a heterodyne receiver: $\mathrm{T_{rec}} > \mathrm{T_{QN}}$. The best modern receivers come within a factor of ~ 3 of the QN limit at low frequencies. For example, the best double-side-band (DSB) receiver temperatures, $\mathrm{T_{rec}}(DSB)$ are: $\mathrm{T_{rec}}(\mathrm{DSB}) \sim 50$ K @ 345 GHz [65], and 75 K at 670 GHz [66]). At frequencies above 1.2 THz, the best receiver temperatures are $\mathrm{T_{rec}}$ (DSB) ~ 1000 k @ 1.3 THz [67], and ~ 3000 K at 2.55 THz [68].

Arguably, one of the most exciting applications of moderate RP THz spectroscopy today is the detection of the THz fine-structure lines from high redshift galaxies. This entails maximizing point source sensitivity over broad bandwidths. Here we compare the relative utility of coherent and incoherent receivers for this work, and demonstrate a compelling case for direct detection at THz frequencies. In terms of the receiver temperature in the presence of background with equivalent noise temperature $\mathrm{T_{bkg}}$, the rms noise temperature at the front end of a coherent receiver, $\Delta\mathrm{T_{FE}}$ in a bandwidth $\Delta\nu$, in integration time, $\Delta\mathrm{t}$ is given by

$$\Delta T_{FE} = a \cdot \frac{(T_{bkg} + T_{rec})}{(\Delta\nu\ \Delta t)^{1/2}}$$

where $\mathrm{a} = 1$ or 2 depending on whether the receiver is configured for single-side-band or double-side-band detection. Clearly if the background is large, and the receiver temperature is small, the effect of the receiver temperature on the overall sensitivity is small. This would be the case for a receiver at 100 GHz, with noise temperature $\sim 3 \cdot \mathrm{T_{QN}} \sim 15$ K, operating from the ground where the combined emissivity of the telescope and the sky might be 15%, i.e., $\mathrm{T_{bkg}} = 0.15{*}300\ \mathrm{K} = 45$ K. However, in space, where $\mathrm{T_{bkg}}$ can approach 2.73 K, and at THz frequencies, where 3 to $15 \cdot \mathrm{T_{QN}} = 150$ to 720 K, the receiver noise can easily dominate that of the background.

In principle, the sensitivity of a direct detection system is only limited by the statistics of the photon arrival rates. For the case of low photon occupancy ($\mathrm{h}\nu/\mathrm{kT} \gg 1$), which applies in the optical band, the noise follows a Poisson distribution, so that the detection of N photons, has an associated noise, $\mathrm{N}^{1/2}$. However, in the THz regime, $\mathrm{h}\nu/\mathrm{kT} \sim 1$, so that the effects of photon bunching must be included. The noise equivalent flux, $\mathrm{NEF_{inc}}[\mathrm{Watts/m^2/Hz^{-1/2}}]$, of a background limited performance (BLIP) spectrometer with cold transmission τ (emissivity 0), operating on a telescope with collecting area, A, efficiency η_{tel}, at temperature T, looking through a sky with transparency η_{sky}, at temperature T, using spectrometer pixels that have point source coupling η_{pixel}, and detective quantum efficiency (DQE) η, is given by [69]

$$NEF_{\mathrm{inc}} = \frac{2h\nu}{(A\eta \cdot \eta_{sky}\eta_{tel}\eta_{pixel})}\left(\frac{2A\Omega}{\Delta t \cdot \lambda^2}\Delta\nu \cdot c_1(1+c_1)\right)^{1/2}$$

where Δt, and $\Delta\nu$ are as before, Ω is the beam solid angle, and $\mathrm{c_1} = \varepsilon \cdot \eta \cdot \tau \cdot \tilde{\mathrm{n}}$ is the product of the warm emissivity ϵ, η, the spectrometer cold transmission τ, and the mode occupation number, $\tilde{\mathrm{n}} = 1/(\exp(\mathrm{h}\nu/\mathrm{kT}) - 1)$. The effective emissivity of the background ϵ, is roughly given by $\varepsilon \sim (1 - \eta_{\mathrm{sky}}) \cdot \eta_{\mathrm{tel}} + (1 - \eta_{\mathrm{tel}})$. The first factor of 2 in this expression arises due to chopping losses of the telescope, while the second factor of 2 is due to the detection of both polarizations of light. The equivalent expression for the heterodyne system is

$$NEF_{coh} = \frac{2 \cdot 2k \cdot \Delta T_{FE}}{(\lambda^2 \cdot \eta_{sky}\eta_{tel}\eta_{taper})}\Delta\nu \cdot \Omega$$

where η_{taper} is the effective fraction of the power in the main beam that couples to a point source due to the edge taper of the beam, and the other parameters are as above. Equating the two expressions and using our equation for ΔT_{FE} above, we have

$$T_{bkd} + T_{rec} = \frac{h\nu}{(ak\eta\tau)}\frac{\eta_{taper}}{\eta_{pixel}} \cdot \frac{2c_1 \cdot (1+c_1)}{1.69\pi}^{1/2}.$$

The factor of 1.69π arises since we assume diffraction limited, Gaussian beams, where $\theta = 1.22\lambda/\mathrm{D}$, and $\Omega = \pi \cdot (\theta/2)^2/\ln(2)$. Here θ is the beam full-width-at-half maximum, and D is the diameter of the telescope primary mirror. We use the ZEUS and ZEUS-2 spectrometers as an example (see below). These spectrometers have $\tau \sim 35\%$, bolometers with $\eta \sim 0.9$, and $\eta_{\mathrm{pixel}} \sim 0.7$. Referring to a single sideband receiver $(\mathrm{a} = 1)$ then for BLIP at 850 GHz at an excellent ground based site $(\eta_{\mathrm{sky}} \sim 58\%, \mathrm{T} = 260$ k) and assuming $\eta_{\mathrm{taper}} = 1$, a coherent single-side-band receiver would need to have a noise temperature of 16 K—*a factor of 2.5 below the quantum noise*

limit—to be equivalent to a background limited grating spectrometer for point source detection. The ZEUS spectrometer delivers sensitivity equivalent to single side band receiver temperatures $\sim 10-30$ K at RPs ~ 1000 [70]. With modern bolometers, it is straight-forward to achieve BLIP in the THz bands for RPs $\sim 10{,}000$, from the ground and airborne facilities so that direct detection systems are the spectrometers of choice for detecting broad spectral lines.

V. Direct Detection THz Spectrometers in Use Today

In this section we describe four current state-of-the-art spectrometers in use at THz frequencies today, including a Fabry–Perot interferometer (SPIFI), a long-slit grating spectrometer (ZEUS), an image slicing grating spectrometer (PACS), and a Fourier transform spectrometer (SPIRE). Each of these spectrometers performs close to the fundamental limits, and due to their unique architecture, has a unique niche of scientific excellence.

A. Comparisons Between Direct Detection Spectrometers

The choice of direct detection spectrometer strongly depends on the science at hand. An FPI or an FTS have much larger luminosity-resolution products at a given R than grating spectrometers that require entrance and exit slits [71]. The FPI/FTS are also readily adapted to imaging spectroscopy so that within limits given by the angular divergence of rays in the beam, large, 2-dimensional focal plane arrays of detectors are easily implemented into these spectrometers creating *spectroscopic imagers*. For detection of a single isolated line over broad regions, the FPI will win over an FTS since, in a BLIP environment, the narrow band of the FPI will deliver much higher sensitivity than the broadband FTS (see below). If, however, one wishes to detect many lines over a very broad range, this sensitivity advantage of the FPI becomes small, and an FTS becomes competitive. However, in terms of raw sensitivity for point source detection, a spectrally multiplexed grating spectrometer is the instrument of choice.

Let us compare a monochrometer (FPI or grating spectrometer) to an FTS of the same RP (see also [72]). We desire to obtain a spectrum with overall bandwidth B, split into N spectral resolution elements, $\Delta\nu : \mathrm{B} = \mathrm{N} \cdot \Delta\nu$. Suppose both instruments have BLIP with noise per resolution element in the monochrometer given by σ_{mono}. The FTS takes in the entire bandwidth, B at the same time, encoding the power of all spectral elements into each step of the interferogram. Since the FTS detector sees the full bandwidth, the noise per unit time is larger than that of the monochrometer by $\sigma_{\mathrm{FTS}} = (\mathrm{B}/\Delta\nu)^{1/2} \cdot \sigma_{\mathrm{mono}} = \mathrm{N}^{1/2} \cdot \sigma_{\mathrm{mono}}$. However, if the monochro-meter is an FPI, one has to scan N resolution elements to deliver the equivalent spectrum as the FTS does in a single inteferogram. Therefore, the total time to deliver the same spectrum is N times longer, so that N interferograms are obtained in the same time as one FPI scan. In this case, then the noise of the FTS spectrum goes down by $\mathrm{N}^{1/2}$, and the two systems are equal.[4] However, a spectrally multiplexed grating spectrometer can have N detectors in the dispersion direction, so that it need not spectrally scan. For this case then, the grating spectrometer is more sensitive than the FTS by $\mathrm{N}^{1/2}$. If, however, the detectors are not background limited—i.e., the noise is independent of bandwidth—the sensitivities become equal again. In this case, the FTS becomes a very interesting choice since it delivers the same N resolution element spectrum as the grating spectrometer, but with just one detector, not N so that it provides a much more effective use of what is often the rarest commodity, the numbers of pixels.

[4]Note that we have ignored the factor of 2 encoding losses of the FTS in this argument. This loss is because the average signal of the interferogram is half the white light signal. However, the FPI will likely have smaller transmission than the FTS due to etalon absorption or the extra filtration needed, so this encoding loss is at least in part cancelled in the comparison.

B. SPIFI—A Bolometer-Based Imaging Fabry-Perot

The **S**outh **P**ole **I**maging **F**abry-**P**erot **I**nterferometer (SPIFI) is the first direct detection imaging spectrometer for use in the submillimeter bands [69], [73], [74]. Unlike previous THz astronomical spectrometers that used either heterodyne techniques, or photoconductors, SPIFI employed bolometers as detectors for the first time. Bolometers have several clear advantages over photoconductors: (1) Ge:Ga photoconductors have DQE's of the order 3 to 26% [75], [76]. In contrast, it is easy to design a bolometer with 50% DQE over very large bandwidths, or by using tuned backshorts, $> 90\%$ DQE over broad ($\lambda/\Delta\lambda \sim 3$) bandwidths [77]. (2) Photoconductors detect photons by discretely generating photoelectrons (or holes). The generation and recombination of these photoelectrons generates shot noise, commonly termed generation recombination (GR) noise. Bolometers are thermal devices so that they do not suffer from GR noise. Therefore, for a given DQE, a bolometer is $\sqrt{2}$ more sensitive than a photoconductor. (3) Bolometers are inherently broadband with nearly constant DQE over this band. Unlike photoconductors, bolometers do not have long wavelength cut-offs due to minimum energy requirements for promotion of electrons from the conduction to valence bands, or poor short-wavelength performance due to strong frequency dependence of ionization cross sections. The photoconductor with the longest wavelength cut-off is stressed Ge:Ga, which has a long-wavelength cut-off near 210 μm or 1.43 THz. The combined sensitivity advantage of bolometers as detectors over photoconductor goes as NEP $\propto 1/2 \cdot (\eta_{\mathrm{PC}}/\eta_{\mathrm{bol}})^{1/2}$, and can be large. As a working demonstration, under similar background conditions, SPIFI at 1.5 THz (200 μm) is a factor of ~ 10 more sensitive than background limited spectrometers that employed stressed Ge:Ga photoconductors as detective devices [2], [31], [75].

SPIFI is an imaging Fabry–Perot interferometer designed to work in the 850 GHz window available to the JCMT on Mauna Kea, and the 1.5 THz window available to the AST/RO telescope at South Pole [69], [73], [74] (Fig. 7). SPIFI employs free-standing metal mesh mirrors in its FPI etalons, which typically deliver reflective finesse $\sim 25-60$, and transmissions $\sim 70-80\%$. SPIFI's RP is fully tunable through changing the order of the high-order FPI (HOFPI), and can be changed from ~ 500 to ~ 10000 in a few minutes while the instrument is mounted on the telescope and operational. SPIFI achieves high spectral purity through the use of a low-order FPI (LOFPI) to select the desired order of the HOFPI, and a fixed bandpass filter to select the desired order of the LOFPI, enabling operation of

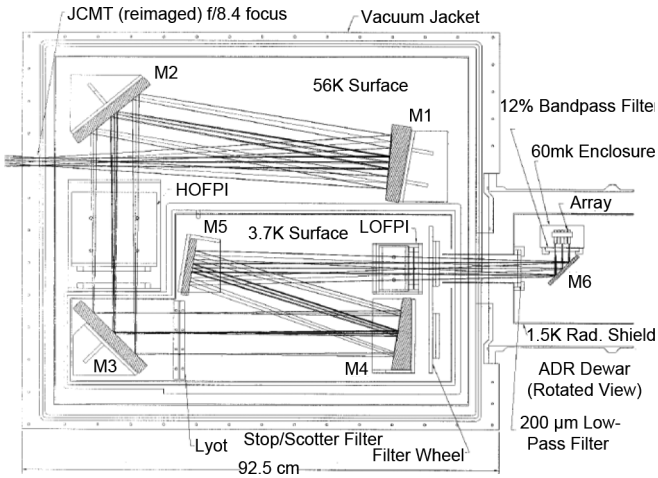

Fig. 7. Optical layout for SPIFI imaging Fabry–Perot [69].

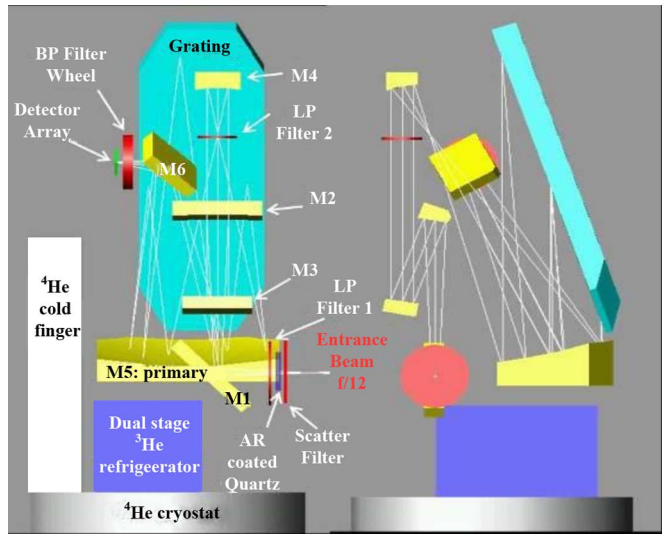

Fig. 8. Optical layout for ZEUS [70]. The grating is in near Littrow configuration.

the LOFPI in orders as high as 10 to 20. The detective devices in SPIFI are a 5×5 array of bolometers from Goddard Space Flight Center (GSFC), that are held at 60 mK in an adiabatic demagnetization refrigerator (ADR). SPIFI was deployed 6 times on the 15 m JCMT. Scientific highlights from these runs included the first detection and mapping of the CO(7-6) line from NGC 253, and the first large-scale map of the CO(7-6) and [CI] lines from the Galactic Center circumnuclear ring [15], [78], [79].

SPIFI was also deployed on the 1.7 m AST/RO telescope at South Pole over the 2004 and 2005 Austral winter. The first season was cut short due to an unexpected rapid depletion of the liquid helium supply for the base, but the second season was quite successful. SPIFI was used in both the 859 GHz and 1.5 THz telluric windows. The highlight of the deployment was the detection and mapping of the [NII] 205 μm line from the Carina star formation region [2], [80]. This was the first detection of this astrophysically important line from the ground, and its strength, when compared with the ISO [CII] and [NII] 122 μm mapping of the nebula demonstrates that the HII regions enveloping the Carina Nebula are low density ($\mathrm{n_e} \sim 30\ \mathrm{cm}^{-3}$), and that only 30% of the observed [CII] line radiation comes from the ionized medium (Fig. 1). Most (70%) of the [CII] radiation arises from PDRs.

SPIFI was close to background limited in both bands of operation: within a factor of 2 at 850 GHz [73], and within a factor of 1.4 at 1.5 THz [74]. The equivalent single-side-band receiver temperature was $\mathrm{T_{rec}(SSB)} \sim 310$ K (40 K DSB) at 850 GHz, and $\mathrm{T_{rec}(SSB)} \sim 610$ K (190 K DSB) at 1.5 THz, which compare quite favorably with the best heterodyne systems today [65], [81].

C. ZEUS/ZEUS-2: Bolometer Based Grating Spectrometers

ZEUS is an echelle grating spectrometer currently configured for operation in the 350 and 450 μm windows available on Mauna Kea [70]. ZEUS employs a 38 cm long R2 echelle grating blazed for 355 μm in 5th order (Fig. 8). As such, the 5th and 4th orders of the echelle are well matched to the 350, and 450 μm (860 and 670 GHz) telluric windows respectively (Fig. 9). The ZEUS grating is operated in near-Littrow mode, and delivers a RP ~ 1000. This RP is near the diffraction limit, and the plate scale was selected so that most $(\sim 50 - 80\%)$ of the flux from a monochromatic point source is coupled into a single pixel. Since extra-galactic line widths are typically $\sim 300\ \mathrm{km/sec}$, this choice of RP, and pixel size optimizes sensitivity for broad lines from point sources—e.g., distant galaxies. ZEUS employs a 1×32 pixel array of planar bolometers from GSFC with backshorts tuned to 400 μm resonance that delivers quantum efficiencies $> 80\%$ over most of the operational band. ZEUS is run with order selecting bandpass filters immediately above the detector array: typically half the array operates in the 350 μm and half in the 450 μm windows. With each pixel corresponding to a resolution element, the instantaneous bandwidth of ZEUS is typically $\sim$ 10 to 14 GHz. ZEUS is very close to background limited, coming within a factor of 1.2 and 1.3 of BLIP at 350 and 450 μm respectively. This performance figure corresponds to $\mathrm{T_{rec}(SSB)} \sim 15$ and 35 K respectively in the centers of the 350 and 450 μm grating orders.

ZEUS has been a regular on the 10.4 m CSO telescope since spring of 2006. Highlights of ZEUS/CSO include the detection of the $^{13}\mathrm{CO}(6-5)$ line from the starburst nucleus of NGC 253—the first detection of the $^{13}\mathrm{CO}(6-5)$ line from an external galaxy, and the first detection of any $^{13}\mathrm{CO}$ transition greater than $\mathrm{J} = 3-2$ from a source beyond the Magellanic clouds [16], and the several high redshift firsts mentioned above including (1) the first detection of the a THz fine-structure line of [OIII] at redshifts beyond 0.05 [63]; (2) the first detection of the [CII] line from the epoch of maximum star formation in the early Universe [8]; (4) the first survey of the [CII] line at high redshift [9]; and (5) the first detection of a THz [NII] line from a source at redshift beyond 0.05 [4]

ZEUS-2 is a multi-color, multi-beam version of ZEUS. The final instrument utilizes two TES bolometer SQUID multi-plexed arrays from NIST [82]. The first is tuned with a $\lambda/4$ back-short to 400 μm, and consists of 280 pixels arranged in a 9 (spatial) $\times$ 40 (spectral) format for use in the 300, 350 and 450 μm windows. The second consists of two sub-arrays. The first has 219 pixels arranged in a

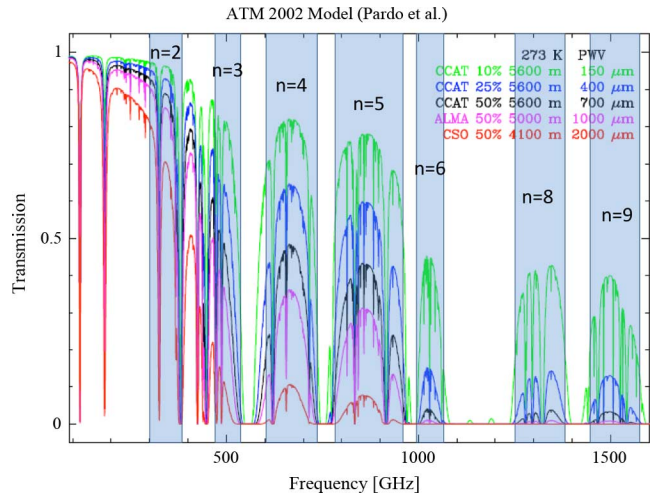

Fig. 9. Echelle orders (n) of ZEUS-2 superposed on telluric transmission plots for CCAT (best10%, 25%, and 50% of nights), at the ALMA site (best 50% of nights), and at the CSO (best 50% of nights). CSO best 25% is similar to ALMA best 50%. ZEUS only accesses $n = 4$ and 5 orders.

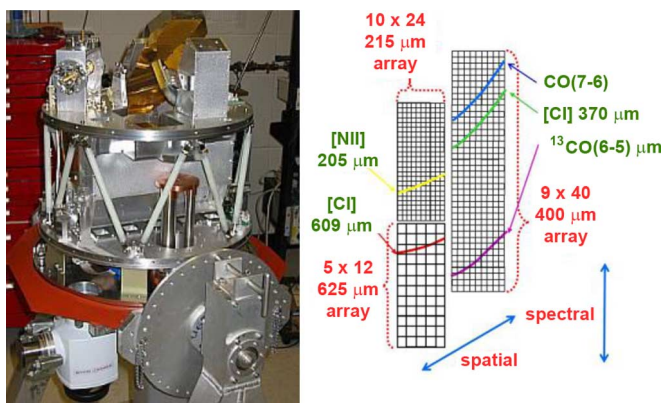

Fig. 10. (left) ZEUS-2 grating, optics, and cryogenics. (right). ZEUS-2 focal plane with grating tuned to simultaneous long-slit spectroscopy in the CO(7-6), ^{13}CO(6 − 5), [NII] and [CI] 370 and 609 μm lines [82].

10 (spatial) × 24 (spectral) format, and is tuned with a $3\lambda/4$ backshort to 215 μm for use in the 200 and 230 μm telluric windows. The second sub-array consists of 56 pixels arranged in a 5 (spatial) × 12 (spectral) format, and is tuned with a $\lambda/4$ backshort to 645 μm. The arrays should achieve DQE > 80% in all bands. ZEUS-2 uses commercially available dual stage ADR and pulse tube cooling systems that not only eliminate the need for expendable cryogens, but also lower the operating temperature of the cold head from 210 mK (with the ZEUS dual stage ^{3}He system) to 100 mK, ensuring greater margin on detector sensitivity.

ZEUS-2 is versatile. By using a filter wheel, the 9th through 2nd orders of the echelle are available for broadband spectroscopy (Fig. 10). For low redshift, resolved objects ZEUS-2 delivers simultaneous spectroscopic imaging of five important astrophysical lines: the [NII] 205 μm, [CI] 609 and 370 μm, CO(7-6) and ^{13}CO(6 − 5) lines (Fig. 10). ZEUS-2 is nearly ready for first light on the CSO in the fall of 2011, and should deliver BLIP with equivalent receiver temperatures of $T_{rec}(SSB) < 30$ K in all bands.

D. PACS

PACS is one of the three science instruments that operate on ESA's 3.5 m Herschel Space Observatory [83]. There are two modes to PACS, an imaging photometer mode, and an integral field spectrometer mode that delivers 16 pixel, Nyquist sampled R ∼ 1700 spectra for each beam over a 5 × 5 beam (47" ×47") field of view. The integral field is obtained by slicing the telescope image plane into 5 rows of 5 beams each with mirrors that direct and map each row independently onto a long grating entrance slit (Fig. 11). A long slit spectrometer is thereby transformed into a compact footprint imaging spectrometer. The detector arrays for PACS are two 16 × 25 pixel arrays of stressed and unstressed Ge:Ga photoconductors that are sensitive to photons between 105–210 and 57–105 μm respectively. The 30 cm long near Littrow mode grating is operated in 1st, 2nd and 3rd order covering 105–210, 72–105, and 55–72 μm respectively. The first order is separated from the 2nd and 3rd orders by a dichroic beam splitter and sent to the stressed Ge:Ga array, while the 2nd and 3rd orders are passed to the unstressed array. Along the short wavelength path a filter wheel enables selection of 2nd or 3rd orders. The detector arrays in PACS deliver peak DQE near 26% [76], resulting in 5σ, 1 hour detection limits of about 3E-18 W/m^2. These values are similar to those of ZEUS on CSO, so that there is a natural synergy between the two systems: redshift 1 to 2 galaxies detectable in [CII] with ZEUS are likely detectable in the [OI] 63 μm or [OIII] (52 or 88 μm) lines with PACS greatly enhancing the science yields of both systems.

The un-obscured views from space, combined with the great sensitivity of PACS has already lead to a number of exciting scientific results, including: (1) the first detection of the [OIII] 52 μm and [OI] 63 μm fine-structure lines from high redshift galaxies [64]; (2) the first survey of local starbursts, Seyfert (AGN), and IR luminous galaxies in the ensemble of far-IR fine-structure lines showing changes in the far-IR line to far-IR continuum ratio suggesting a shift to a higher efficiency mode of star formation in the most luminous systems [84]; and (3) the first evidence for massive molecular outflows in ULIRG galaxies that may quench their star formation activity [85].

E. SPIRE

SPIRE is the second direct detection instrument on the HSO [86]. Like PACS, SPIRE contains both imaging photometer, and imaging spectrometer modules. The spectrometer is an FTS in a Mach–Zehnder configuration. The FTS contains twin interferometer arms modulated by the same scan mechanism, so that spectra are simultaneously obtained from two different bolometer arrays that are arranged to spatially overlap on the sky (Fig. 12). The first array covers the 194–313 μm band with 37 bolometers, and the second covers the 303–671 μm band with 19 bolometers. The bolometer arrays consist of discrete "spider-web" bolometers fed by single mode conical feed horns. These open architecture arrays deliver very low NEPs at the base temperature of 0.3 K delivered by the ^{3}He refrigerator plus exceptionally low susceptibility to cosmic ray hits [87]. The FTS resolution element is fully tunable from 2–0.04 cm^{-1}

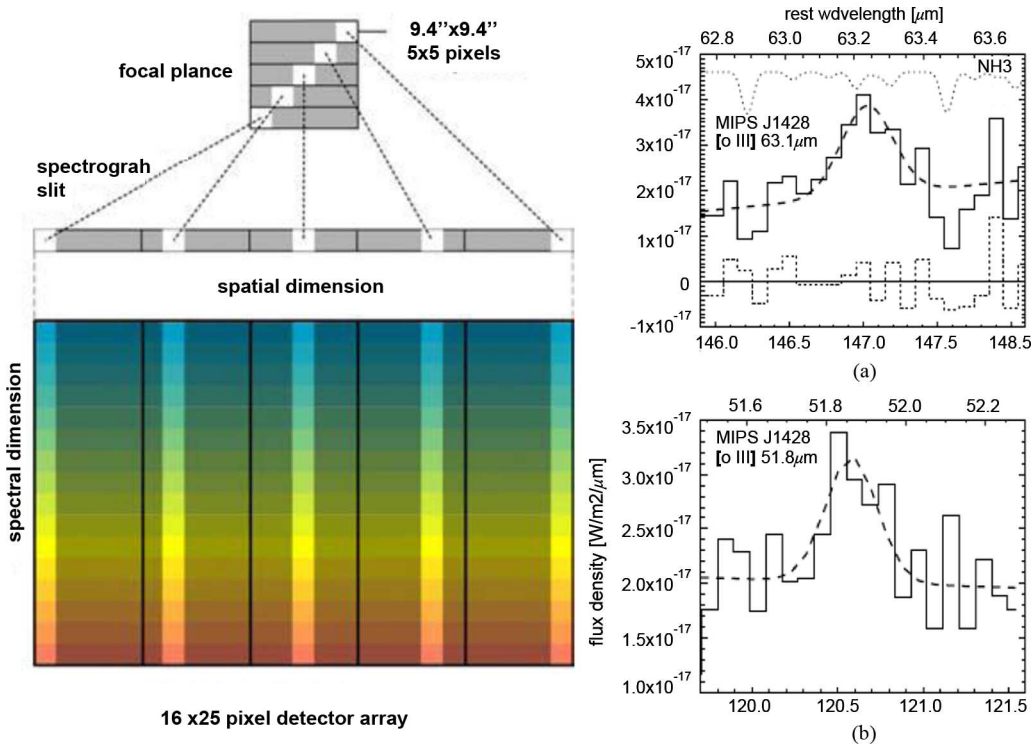

Fig. 11. (left) Mapping the focal plane image onto a long slit within the PACS spectrometer. (right) [OI] 63 μm and [OIII] 52 μm fine-structure lines detected by PACS from the $z = 1.325$ starburst galaxy MIPS J142824 [64].

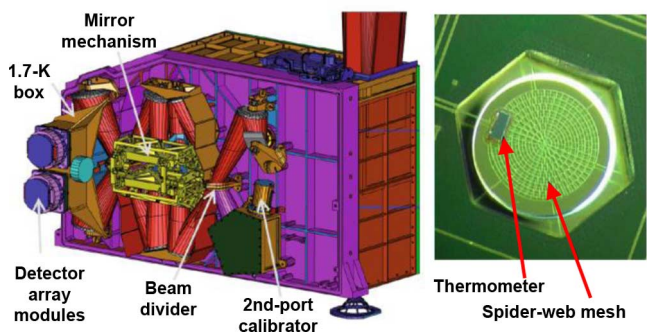

Fig. 12. (left) SPIRE interferometer optical path (right) close-up of a SPIRE spider-web bolometer showing the mesh architecture of the absorber, and the thermometer. The thermometer is $10 \times 100 \times 300$ μm in size [86], [87].

(unapodized), so that the highest RP varies from 1300 and 370 from the shortest to longest wavelengths.

The unique SPIRE niche is very broadband moderate resolution spectroscopy, underscored by the un-obscured vision of the HSO in space. SPIRE therefore has observed a variety of lines for the first time, or the first time from an external galaxy (Fig. 5). The broad bandwidth also enables simultaneous measurements of many rotational transitions of CO from galaxies, characterizing both PDRs and XDRs, and enabled the first detailed studies of water line emission from external galaxies [53]. SPIRE has performed far better than pre-launch expectations, delivering the requisite sensitivity to detect redshifted fine-structure lines at $z > 2$ as well [88], [89].

VI. Future Prospects

There are many new astrophysical discoveries being made right now using low resolution THZ spectroscopy boosted by both developments in ground based instrumentation, and the spectacular success of Herschel in space. The future is even more exciting. The SOFIA facility is just now undergoing its first science flights, the enormously powerful ALMA facility has just released its call for first science proposals, and looming on the near horizon are the 25 m CCAT telescope, and the 3.5 m SPICA space mission. We briefly discuss the scientific prospects for each of these facilities

A. SOFIA

The Stratospheric Observatory for Infrared Astronomy (SOFIA) contains a 2.5 m telescope in a modified Boeing 747 SP [90] (Fig. 13). Like CCAT, SOFIA is a readily accessible evolving observatory under which we may develop the next generation of instrumentation, taking advantage of the latest technologies. A THz image slicing spectrometer, FIFI-LS is developed for SOFIA, and will be deployed in 2012 [91]. FIFI-LS is similar in many respects to PACS, but the SOFIA facility is better optimized for mapping experiments, so that for FIFI-LS/SOFIA we may expect, for example, large format mapping programs of nearby resolved galaxies revealing the roles of spiral arms and bars in compression of the ISM and ignition of the next generation of star formation in spiral galaxies. New THz spectrometers will be deployed in future years on SOFIA including heterodyne arrays, and bolometer based direct detection systems enabling new science. After Herschel cryogens expire, and before SPICA is launched, SOFIA will be

Fig. 13. SOFIA is a Boeing 747 SP modified to carry an open port 2.7 m telescope (chopped aperture 2.5 m), that enables routine access to the highest THZ frequencies [90].

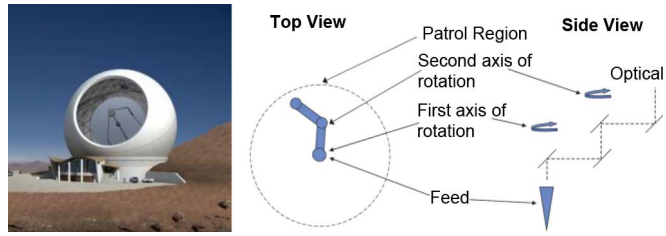

Fig. 14. (left) CCAT concept. (right) Simple rotating periscope design for converting a long slit, or stacked Z-Spec-like spectrometer into a multi-object spectrometer. Each beam is coupled into the focal plane by the periscope design, and assigned a "patrol-area" of the focal plane [95].

the only facility from which high frequency THz observations can be made.

B. CCAT

CCAT is a 25 m submm telescope under design by a consortium of universities led by Cornell University that includes Cornell, Caltech, the Universities of Colorado, Bonn, and Cologne, and a consortium of Canadian Universities [92]. CCAT is to have an exceptionally good surface (10 μm RMS), and to be sited near the peak of Cerro Chajnantor in the northern Atacama desert, at an elevation of 5600 m so that CCAT will deliver exceptional sensitivity in the submm bands. Wide-field surveys in the THz continuum with CCAT promise to nearly fully resolve the THz background radiation into its constituent sources. In a 2 year survey, CCAT will detect hundreds of thousands of high redshift galaxies enabling statistically significant studies of star formation to redshifts approaching 10—looking back into time to within 500 million years of the Big Bang. These continuum surveys will discover the sources, but to fully understand the star—***and galaxy***— formation process in the early Universe will require direct detection spectroscopy in the various lines as outlined above. This is surprisingly straight-forward. The observed brightness of the [CII] line in redshift 1–2 star forming galaxies [8], [9] is consistent with a [CII] to underlying THz dust continuum ratio of 10:1. Since continuum sensitive cameras will have bandwidths of 10%, or RP $\sim$ 10, and grating spectrometers optimized for line detection have RP $\sim$ 1000, the sensitivity ratio is $(1000/10)^{1/2} = 10$. Therefore, it is as easy to detect the [CII] line as it is the underlying continuum, provided the source redshift falls into the telluric windows. CCAT should detect 1000's of galaxies per square degree in [CII] and other THz fine-structure lines. For detection of sources with unknown redshifts, very large bandwidths are desired. This can be achieved with free space grating spectrometers in low (1st or 2nd) order, or a THz version of Z-Spec. Z-Spec is a mm wave direct detection spectrometer that achieves very broad detection bandwidth using a curved diffraction grating in a parallel-plate waveguide [93], [94]. Either system can deliver detection $\mathrm{bandwidth} \sim \nu/2$ with good optical efficiency. Since sources will be detected at the confusion limit on the sky a multi-object direct detection spectrometer is of importance. Simple concepts for feeding multiple beams into spectroscopes exist. For example, a quasi-optical design involving twin elbowed periscopes [95] (Fig. 14), could $\mathrm{feed} > 10$ beams into a long slit spectrometer, or a stack of THz frequency Z-Spec-like spectrometers thereby creating a multi-object system.

Due to its large aperture, exceptional surface, exceptional site, and the use of very broad bandwidth direct detection multiband spectrometers, CCAT can detect THz lines from distant galaxies at the rate of tens per hour. Once detected, particularly interesting sources can be delivered to ALMA (see below) for follow-up observations with its exquisite velocity resolved imaging capabilities.

C. SPICA

SPICA is a 3.2 m telescope cooled to below 6 K to be launched by the Japanese space agency, JAXA as early as 2020 [96]. With its large, very cold aperture in space, SPICA promises to deliver unrivaled sensitivity in the high frequency THz bands. At present the SAFARI spectrometer to be delivered by ESA is the baseline THz spectrometer [97]. SAFARI covers the 30–210 μm band with tunable RP $\sim$ 10 to 10,000, Mach–Zehnder imaging FTS, and should deliver sensitivities 20 to 30 times better than PACS/Herschel. There may also be an instrument from NASA on SPICA. A concept based on a combination of cross-dispersed free space spectrometers like the Spitzer IRS modules [98], and wave-guide spectrometers both operated with TES bolometers, called BLISS is under study [99]. BLISS will operate in the 38 to 433 μm regime. The goal is for BLISS to come within a factor of two of the background limit determined by cosmic backgrounds at a RP $\sim$ 700. This would yield point source sensitivities 300 times better than Hershel, opening up the most distant galaxies for spectroscopic study in the THz bands. For instance, BLISS/SPICA should be able to detect the [OI] 63 μm line emission from a ULIRG galaxy at $z = 6$ (5σ, 2 hours), or to within 1 Gyr of the Big Bang.

D. ALMA

The Atacama Large Millimeter/Submillimeter Array (ALMA) is a large interferometer being built on the Chajnantor plateau in the Atacama Desert in northern Chile by an international collaboration including Europe, East Asia, and North America in cooperation with the Republic of Chile. A primary science goal is detection of the [CII] line from a Milky Way-like galaxy at $z \sim 5$ in less than 24 hours observing time. When completed ALMA will consist of 54-12 m and 12-7 m high surface accuracy antennas linked for interferometry. Its exceptionally high (5000 m elevation) and dry site enables

TABLE II
ALMA RECEIVER BANDS.

Band Number	Frequency Range (GHz)	Band Number	Frequency Range (GHz)
1	31.3-45.0	6	211-275
2	67-90	7	275-373
3	84-116	8	385-500
4	125-163	9	602-720
5	163-211	10	787-950

routine observations in the short submm bands. The ALMA facility is designed to operate from 31.3 GHz to 950 GHz, sub-divided into 10 bands based on technology and telluric window matches (Table II). At its full potential, each ALMA antenna can be equipped with up to 10 very low noise receivers (e.g., [65], [66]). With the enormous collecting area, low $T_{\rm rec}$ and baselines as long as 16 km, ALMA will achieve unmatched sensitivity in its bands, for line detection at spatial resolutions as small as 6 milli-arcsec at 675 GHz. Early science programs involving 16 antennas operating in bands 3, 6, 7 and 9 are to begin in the fall of 2011.

E. Combined Facilities: Star and Galaxy Formation

The pioneering work outlined in Section III above brings an understanding of the enormous diagnostic potential of the THz fine-structure lines for astrophysical research. Recent work demonstrates the potential for direct detection spectroscopic studies of near and distant galaxies (Section IV). With the combined power of the new instrumentation and facilities (Sections V and VI), one can address fundamentally important questions about the history of star and galaxy formation in the Universe. Questions include: (1) How do stellar populations evolve over time? Stellar structure models predict an evolution in the intial mass function over the history of the Universe in the sense that the distribution of stellar masses at birth is skewed towards more massive stars at early times, which should result in observable changes in the hardness of UV radiation fields. (2) There was clearly a link between the growth of stellar populations and supermassive black holes at the centers of galaxies in the early Universe. This link is manifest today as correlation with black hole mass and the velocity dispersion of the stellar bulge in local galaxies [100], [101]. What is the star formation-AGN feedback mechanism that promotes this link? (3) How does star formation evolve over time? Does the star formation mode change, both in efficiency and scale from earliest times until the present?

These questions can be addressed through coordinated campaigns with near future facilities. CCAT will detect hundreds of thousands of new sources enabling statistically significant population studies as a function of time back to within a billion years of the Big Bang. With broadband CCAT spectrometers, the redshifts for these sources will be determined through the bright THz fine-structure lines. Lines observed through the telluric windows will be supplemented by spectroscopic work in spectral regimes obscured by telluric water vapor (at least for the brighter sources) using high sensitivity spectrometers on SOFIA. The combined line studies will constrain the physical conditions of the ISM and ambient radiation fields for these sources. How does the stellar population of IR luminous galaxies evolve over time? With its small beam, CCAT sources will have positional coordinates adequate for detailed follow-up with the high sensitivity and high spatial resolution of ALMA. Do the THZ lines arise from the AGN/torus (localized emission) or from starbursts (extended)? How extended are the starburst? Are they stimulated by galaxy-galaxy collisions? Finally, the sensitivity of SPICA enables detection of many shorter wavelength lines that have critical diagnostic features. For example, SPICA enables detection of the [OIV] 26 μm line from these high redshift sources. This line, when compared with the THz [OIII] lines is a definitive measure of AGN activity. What are the relative contributions of star formation and AGN to source luminosity? The synergies between the new facilities will usher in a golden age of discovery through THz spectroscopy.

REFERENCES

[1] B. D. Savage and K. R. Sembach, "Interstellar abundances from absorption-line observations with the hubble space telescope," in *Annual Reviews of Astron. Astrophys.*, G. Burbidge and A. Sandage, Eds. Palo Alto, CA: Annual Reviews, Inc., 1996, vol. 34, pp. 279–329.

[2] T. E. Oberst *et al.*, "Detection of the 205 μm [N II] line from the Carina Nebula," *Astrophys. J.*, vol. 652, pp. L125–L128, Dec. 2006.

[3] R. H. Rubin, "Models of H II regions—Heavy element opacity, variation of temperature," *Astrophys. J. Supplement Series*, vol. 57, pp. 349–349, Feb. 1985.

[4] C. Ferkinhoff *et al.*, "First detections of [N II] 122 μm line at $z > 0.04$: Demonstrating the utility of the line for studying galaxies at high redshift," *Astrophys. J. Lett.*, May 2011, submitted for publication.

[5] D. J. Hollenbach and A. G. G. M. Tielens, "Photodissociation regions in the interstellar medium of galaxies," *Rev. Mod. Phys.*, vol. 71, pp. 173–230, Jan. 1999.

[6] M. G. Wolfire, A. G. G. M. Tielens, and D. Hollenbach, "Physical conditions in photodissociation regions—Applicationto galactic nuclei," *Astrophys. J.*, vol. 358, pp. 116–131, Jul. 1990.

[7] G. J. Stacey, N. Geis, R. Genzel, J. B. Lugten, A. Poglitsch, A. Sternberg, and C. H. Townes, "The 158 micron [C II] line—A measure of global star formation activity in galaxies," *Astrophys. J.*, vol. 373, pp. 423–444, Jun. 1991.

[8] S. Hailey-Dunsheath, T. Nikola, G. J. Stacey, T. E. Oberst, S. C. Parshley, D. J. Benford, J. G. Staguhn, and C. E. Tucker, "Detection of the 158 μm [C II] transition at $z = 1.3$: Evidence for a galaxy-wide starburst," *Astrophys. J.*, vol. 714, pp. L162–L166, May 2010.

[9] G. J. Stacey, S. Hailey-Dunsheath, C. Ferkinhoff, T. Nikola, S. C. Parshley, D. J. Benford, J. G. Staguhn, and N. Fiolet, "A 158 μm [C II] line survey of galaxies at $z \sim 1-2$: An indicator of star formation in the early universe," *Astrophys. J.*, vol. 724, pp. 957–974, Dec. 2010.

[10] G. J. Stacey, P. J. Viscuso, C. E. Fuller, and N. T. Kurtz, "The 157-micron [C II] luminosity of the galaxy. II—The presence of knotlike features in the [C II] emission," *Astrophys. J.*, vol. 289, pp. 803–806, Feb. 1985.

[11] E. L. Wright *et al.*, "Preliminary spectral observations of the galaxy with a 7 deg beam by the cosmic background explorer (COBE)," *Astrophys. J.*, vol. 381, pp. 200–209, Nov. 1991.

[12] M. L. Luhman, S. Satyapal, J. Fischer, M. G. Wolfire, E. Sturm, C. Dudley, D. Lutz, and R. G. Genzel, "The [C II] 158 micron line deficit in ultraluminous infrared galaxies revisited," *Astrophys. J.*, vol. 594, pp. 758–775, Sep. 2003.

[13] J. Wagg, C. L. Carilli, D. J. Wilner, P. Cox, C. De Breuck, K. Menten, D. A. Riechers, and F. Walter, "[C II] line emission in BRI 1335–0417 at $z = 4.4$," *Astron. Astrophys.*, vol. 519, pp. L1–L4, Sep. 2010.

[14] J. R. Brauher, D. A. Dale, and G. Helou, "A compendium of far-infrared line and continuum emission for 227 galaxies observed by the infrared space observatory," *Astrophys. J. Supplement Series*, vol. 178, pp. 280–301, Oct. 2008.

[15] C. M. Bradford, T. Nikola, G. J. Stacey, A. D. Bolatto, J. M. Jackson, M. L. Savage, J. A. Davidson, and S. J. Higdon, "CO($J = 7-6$) observations of NGC 253: Cosmic-ray-heated warm molecular gas," *Astrophys. J.*, vol. 586, pp. 891–901, Apr. 2003.

[16] S. Hailey-Dunsheath, T. Nikola, G. J. Stacey, T. E. Oberst, S. C. Parshley, C. M. Bradford, P. A. R. Ade, and C. E. Tucker, "Detection of the ^{13}CO$J = 6 - 5$ transition in the starburst galaxy NGC 253," *Astrophys. J.*, vol. 689, pp. L109–L112, Dec. 2008.

[17] P. Papadopoulos, K. Isaak, and P. van der Werf, "CO $J = 6 - 5$ in Arp 220: Strong effects of dust on high-J CO lines," *Astrophys. J.*, vol. 711, pp. 757–763, Mar. 2010.

[18] T. Nikola, S. Hailey-Dunsheath, G. J. Stacey, T. E. Oberst, D. J. Benford, J. G. Staguhn, and C. E. Tucker, "Mid-J CO observations of IR luminous galaxies," *Astrophys. J.*, 2011, submitted for publication.

[19] A. I. Harris, J. Stutzki, U. U. Graf, A. P. G. Russell, R. Genzel, and R. E. Hills.Ha, "First observations of the CO $J = 6 - 5$ transition in starburst galaxies," *Astrophys. J.*, vol. 382, pp. L75–L79, Dec. 1991.

[20] J. S. Ward, J. Zmuidzinas, A. I. Harris, and K. G. Isaak, "A ^{12}CO $J = 6-5$ map of M82: The significance of warm molecular gas," *Astrophys. J.*, vol. 587, pp. 171–185, Apr. 2003.

[21] V. Petrosian, "Infrared line emission from H II regions," *Astrophys. J.*, vol. 159, pp. 833–846, Mar. 1970.

[22] A. Dalgarno and R. McCray, "Heating and ionization of HI regions," in *Annual Reviews of Astron. Astrophys.*. Palo Alto: Annual Reviews, Inc., 1972, vol. 10, pp. 375–426.

[23] J. P. Simpson, "Spectrophotometry of the Orion Nebula," *Publications of the Astronomical Society of the Pacific*, vol. 85, pp. 479–492, Oct. 1973.

[24] D. B. Ward, B. Dennison, G. Gull, and M. Harwit, "Detection of the [O III] 88.16-micron line in M17," *Astrophys. J.*, vol. 202, pp. L31–L32, Nov. 1975.

[25] G. Melnick, G. E. Gull, and M. Harwit, "Observations of the 51.8 micron [O III] emission line in Orion," *Astrophys. J.*, vol. 222, pp. L137–L140, Jun. 1978.

[26] G. Melnick, G. E. Gull, and M. Harwit, "Observations of the 63 micron [O I] emission line in the Orion and Omega Nebulae," *Astrophys. J.*, vol. 227, pp. L29–L33, Jan. 1979.

[27] G. J. Stacey, S. D. Smyers, N. T. Kurtz, and M. Harwit, "Observations of the 145.5 micron [OI] emission line in the Orion Nebula," *Astrophys. J.*, vol. 265, pp. L7–L11, Feb. 1983.

[28] R. W. Russell, G. Melnick, G. E. Gull, and M. Harwit, "Detection of the 157 micron /1910 GHz [C II] emission line from the interstellar gas complexes NGC 2024 and M42," *Astrophys. J.*, vol. 240, pp. L99–L103, Sep. 1980.

[29] A. F. M. Moorwood, P. Salinari, I. Furniss, R. E. Jennings, and K. J. King, "Infrared spectroscopy with a balloon borne Michelson interferometer. II observation of [O III], [O I], and [N III] fine structure lines in H II regions," *Astron. Astrophys.*, vol. 90, pp. 304–310, Oct. 1980.

[30] M. Anderegg, A. F. M. Moorwood, P. Salinari, I. Furniss, R. E. Jennings, K. J. King, W. A. Towlson, and T. E. Venis, "Infrared spectroscopy with a balloon-borne Michelson interferometer. I—Instrumentation and performance," *Astron. Astrophys.*, vol. 82, pp. 86–92, Feb. 1980.

[31] S. W. J. Colgan, M. R. Haas, E. F. Erickson, R. H. Rubin, J. P. Simpson, and R. W. Russell, "Detection of the [N II] 122 and 205 micron lines—Densities in G333.6–0.2," *Astrophys. J.*, vol. 413, pp. 237–241, Aug. 1993.

[32] T. G. Phillips, P. J. Huggins, T. B. H. Kuiper, and R. E. Miller, "Detection of the 610 micron /492 GHz line of interstellar atomic carbon," *Astrophys. J.*, vol. 238, pp. L103–L106, Jun. 1980.

[33] D. T. Jaffe, A. I. Harris, M. Silber, R. Genzel, and A. L. Betz, "Detection of the 370 micron ^{3}P$_2$-^{3}P$_1$ fine-structure line of [CI]," *Astrophys. J.*, vol. 209, pp. L59–L62, Mar. 1985.

[34] H. Shibai *et al.*, "Large-scale [C II] 158 micron emission from the galaxy," *Astrophys. J.*, vol. 374, pp. 522–532, Jun. 1991.

[35] I. Furniss, R. E. Jennings, K. J. King, J. F. Lightfoot, R. J. Emery, D. A. Naylor, and B. Fitton, "Observations of M42 in the [O III] 52 and 88-micron lines, the [O I] 63-micron line, and the [NIII] 57-micron line," *Monthly Notices Roy. Astronom. Soc.*, vol. 202, pp. 859–865, Mar. 1983.

[36] D. M. Watson, R. Genzel, C. H. Townes, M. W. Werner, and J. W. V. Storey, "Detection of far-infrared [O I] and [O III] emission from the galaxy M82," *Astrophys. J.*, vol. 279, pp. L1–L4, Apr. 1984.

[37] M. K. Crawford, R. Genzel, C. H. Townes, and D. M. Watson, "Far-infrared spectroscopy of galaxies—The 158 micron C^+ line and the energy balance of molecular clouds," *Astrophys. J.*, vol. 291, pp. 755–771, Apr. 1985.

[38] S. C. Madden, N. Geis, R. Genzel, F. Herrmann, J. Jackson, A. Poglitsch, G. J. Stacey, and C. H. Townes, "158 micron [C II] mapping of NGC 6946—Probing the atomic medium," *Astrophys. J.*, vol. 407, pp. 579–587, Apr. 1993.

[39] P. B. Duffy, E. F. Erickson, M. R. Haas, and J. R. Houck, "Far-infrared spectroscopy of star formation regions in M82," *Astrophys. J.*, vol. 315, pp. 68–73, Apr. 1987.

[40] P. Carral, D. J. Hollenbach, S. D. Lord, S. W. J. Colgan, M. R. Haas, R. H. Rubin, and E. F. Erickson, "The interstellar medium in the starburst regions of NGC 253 and NGC 3256," *Astrophys. J.*, vol. 423, pp. 223–236, Mar. 1993.

[41] S. D. Lord, D. J. Hollenbach, M. R. Haas, R. H. Rubin, S. W. J. Colgan, and E. F. Erickson, "Interstellar properties of a dual nuclear starburst: Far-infrared spectroscopy of M82," *Astrophys. J.*, vol. 465, pp. 703–716, Jul. 1996.

[42] R. Barvainis, P. Maloney, R. Antonucci, and D. Alloin, "Multiple CO transitions, C I, and HCN from the Cloverleaf Quasar," *Astrophys. J.*, vol. 484, pp. 695–701, Aug. 1997.

[43] E. Gonzalez-Alfonso, H. A. Smith, J. Fischer, and J. Chernicharo, "The far-infrared spectrum of Arp 220," *Astrophys. J.*, vol. 613, pp. 247–261, Sep. 2004.

[44] C. J. Skinner, H. A. Smith, E. Sturm, M. J. Barlow, R. J. Cohen, and G. J. Stacey, "A starburst origin of the OH-megamaser emission from the galaxy Arp220," *Nature*, vol. 386, pp. 472–474, Apr. 1997.

[45] J. W. V. Storey, D. M. Watson, and C. H. Townes, "Detection of interstellar OH in the far-infrared," *Astrophys. J.*, vol. 244, pp. L27–L30, Feb. 1981.

[46] G. J. Stacey, J. B. Lugten, and R. Genzel, "Detection of interstellar CH in the far-infrared," *Astrophys. J.*, vol. 313, pp. 859–866, Feb. 1987.

[47] J. B. Lugten, "Velocity Resolved Far-Infrared Spectroscopy of Galactic Sources," Ph.D., University of California, Berkeley, California, 1987.

[48] B. T. Draine, *Physics of the Interstellar and Intergalactic Medium*. Princeton, NJ: Princeton University Press, 2011, pp. 1–10.

[49] J. W. Colbert *et al.*, "ISO LWS spectroscopy of M82: A unified evolutionary model," *Astrophys. J.*, vol. 511, pp. 721–729, Feb. 1999.

[50] J. Fischer *et al.*, "ISO FAR-IR spectroscopy of IR-bright galaxies and ULIRGs," *Astrophys. Space Sci.*, vol. 266, pp. 91–98, Jan. 1999.

[51] R. Genzel *et al.*, "What powers ultraluminous IRAS Galaxies?," *Astrophys. J.*, vol. 498, pp. 579–605, May 1998.

[52] P. Van der Werf *et al.*, "Black hole accretion and star formation as drivers of gas excitation and chemistry in Markarian 231," *Astron. Astrophys.*, vol. 518, pp. 221–225, Jul. 2010.

[53] A. González-Alfonso *et al.*, "Herschel observations of water vapour in Markarian 231," *Astron. Astrophys.*, vol. 518, pp. 226–230, Jul. 2010.

[54] R. Meijerink, M. Spaans, and F. P. Israel, "Diagnostics of irradiated dense gas in galaxy nuclei. II. A grid of XDR and PDR models," *Astron. Astrophys.*, vol. 461, pp. 793–811, Jan. 2007.

[55] J.-L. Puget, A. Abergel, J.-P. Bernard, F. Boulanger, W. B. Burton, F.-X. Desert, and D. Hartmann, "Tentative detection of a cosmic far-infrared background with COBE," *Astron. Astrophys.*, vol. 308, pp. L5–L8, Apr. 1996.

[56] D. J. Fixsen, E. Dwek, J. C. Mather, C. L. Bennett, and R. A. Shafer, "The spectrum of the extragalactic far-infrared background from the COBE FIRAS observations," *Astrophys. J.*, vol. 508, pp. 123–128, Nov. 1998.

[57] M. J. Devlin *et al.*, "Over half of the far-infrared background light comes from galaxies at $z > 1.2$," *Nature*, vol. 458, pp. 737–739, Apr. 2009.

[58] I. Smail, S. C. Chapman, A. W. Blain, and R. J. Ivison, "The rest-frame optical properties of SCUBA galaxies," *Astrophys. J.*, vol. 616, pp. 71–85, Nov. 2004.

[59] A. Weiß, C. Henkel, D. Downes, and F. Walter, "Gas and dust in the Cloverleaf Quasar at redshift 2.5," *Astron. Astrophys.*, vol. 409, pp. L41–L45, Oct. 2003.

[60] R. Maiolino *et al.*, "First detection of [C II] 158 μm at high redshift: Vigorous star formation in the early universe," *Astron. Astrophys.*, vol. 440, pp. L51–L54, Sep. 2005.

[61] D. Iono *et al.*, "A detection of [C II] line emission in the $z = 4.7$ QSO BR 1202–0725," *Astrophys. J.*, vol. 645, pp. L97–L100, Jul. 2006.

[62] R. Maiolino, P. Caselli, T. Nagao, M. Walmsley, C. De Breuck, and M. Meneghetti, "Strong [C II] emission at high redshift," *Astron. Astrophys.*, vol. 500, pp. L1–L4, Jun. 2009.

[63] C. Ferkinhoff, S. D. Hailey-Dunsheath, T. Nikola, S. C. Parshley, G. J. Stacey, D. J. Benford, and J. G. Staguhn, "First detection of the [O III] 88 μm line at high redshifts: Characterizing the starburst and narrow-line regions in extreme luminosity systems," *Astrophys. J.*, vol. 714, pp. L147–L151, May 2010.

[64] E. Sturm *et al.*, "Herschel-PACS spectroscopy of IR-bright galaxies at high redshift," *Astron. Astrophys.*, vol. 518, pp. 195–198, Jul. 2010.

[65] C. Risacher *et al.*, "A 0.8 mm heterodyne facility receiver for the APEX telescope," *Astron. Astrophys.*, vol. 454, pp. L17–L20, Aug. 2008.

[66] A. M. Baryshev *et al.*, "ALMA band 9 cartridge," in *Proc. 19th Int. Sym. Space Terahertz Technol.*, 2008, pp. 258–262.
[67] M. C. Wiedner *et al.*, "First observations with CONDOR, a 1.5 THz heterodyne receiver," *Astron. Astrophys.*, vol. 454, pp. L33–L36, Aug. 2008.
[68] R. Guesten *et al.*, "GREAT -German REceiver for Astronomy at Teraherz Frequencies," [Online]. Available: www.sofia.usra.edu/Science/instruments/instruments_great.html
[69] C. M. Bradford, "The Warm, Dense Gas in the Central Two Parsecs of the Galaxy: Observations With SPIFI, a New Direct-Detection Submillimeter Spectrometer," Ph.D. dissertation, Cornell Univ., Ithaca, NY, 2000.
[70] S. Hailey-Dunsheath, "Probing Star Formation at Low and High Redshift With ZEUS, a New Submillimeter Grating Spectrometer," Ph.D., Cornell University, New York, 2009.
[71] P. Jacquinot, "The luminosity of spectrometers with prisms, gratings, or Fabry-Perot etalons," *J. Opt. Soc. Amer.*, vol. 44, pp. 761–765, 1954.
[72] D. M. Watson, "Shock Waves and Mass Outflow in the Orion Molecular Cloud: Observations of Far-Infrared Emission Lines of Carbon Monoxide, Hydroxyl and Ammonia," Ph.D. dissertation, Univ. California, Berkeley, 1982.
[73] C. M. Bradford, G. J. Stacey, M. R. Swain, T. Nikola, A. D. Bolatto, J. M. Jackson, M. L. Savage, J. A. Davidson, and P. A. R. Ade, "SPIFI: A direct-detection imaging spectrometer for submillimeter wavelengths," *Appl. Opt.*, vol. 41, pp. 2561–2574.
[74] T. E. Oberst, "Submillimeter Spectroscopy of the Carina Nebula: Observations, Operations and Upgrades of the South Pole Imaging Fabry-Perot Interferometer," Ph.D. dissertation, Cornell Univ., Ithaca, NY, 2009.
[75] G. J. Stacey, J. W. Beeman, E. E. Haller, N. Geis, A. Pogitsch, and M. Rumitz, "Stressed and unstressed Ge:Ga detector arrays for airborne astronomy," *Int. J. Infrared Millimeter Waves*, vol. 13, pp. 1689–1707, Nov. 1992.
[76] A. Poglitsch *et al.*, PACS Observers Manual Internet, 2007 [Online]. Available: http://www.iac.es/proyecto/herschel/pacs/pacs_om.pdf
[77] G. H. Reike, *Detection of Light From the Ultraviolet to the Submillimeter*. Cambridge, U.K.: Cambridge Univ. Press, 1994, pp. 250–252.
[78] C. M. Bradford, G. J. Stacey, T. Nikola, A. D. Bolatto, J. M. Jackson, M. L. Savage, and J. A. Davidson, "Warm molecular gas traced with CO $J = 7 - 6$ in the galaxy's central 2 parsecs: Dynamical heating of the circumnuclear disk," *Astrophys. J.*, vol. 623, pp. 866–876, Apr. 2005.
[79] D. Brisbin *et al.*, "A second ZEUS survey of [C II] in the redshift interval from 1 to 2," *Astrophys. J.*, 2011, submitted for publication.
[80] T. E. Oberst, S. C. Parshley, T. Nikola, G. J. Stacey, A. Löhr, A. P. Lane, A. A. Stark, and J. Kamenetzky, "A 205 μm [N II] map of the Carina Nebula," *Astrophys. J.*, 2011.
[81] S. Yngvesson *et al.*, G. Narayanan, Ed., "Upgrade to the TREND laser LO at the South Pole Station," in *Proc. 15th Int. Symp. Space THz Technol.*, 2004, pp. 365–372.
[82] C. Ferkinhoff, T. Nikola, S. C. Parshley, G. J. Stacey, K. D. Irwin, H.-M. Cho, and M. Halpern, "ZEUS-2: A second generation submillimeter grating spectrometer for exploring distant galaxies," in *SPIE Conference Series*, Jul. 2010, vol. 7741, pp. 77410Y-77410Y-14–77410Y-77410Y-14.
[83] A. Poglitsch *et al.*, "The photodetector array camera and spectrometer (PACS) on the Herschel Space Observatory," *Astron. Astrophys.*, vol. 518, pp. 9–20, Jul. 2010.
[84] J. Gracia-Carpio *et al.*, "Far-infrared line deficits in galaxies with extreme $L_{\rm FIR}/M_{(H2)}$ ratios," *Astrophys. J.*, vol. 728, pp. L7–L11, Feb. 2007.
[85] E. Sturm *et al.*, "Massive molecular outflows and Negative feedback in ULIRGs observed by Herschel-PACS," *Astron. Astrophys.*, vol. 733, pp. L16–L20, May 2011.
[86] M. Griffin *et al.*, "The Herschel-SPIRE instrument and its in-flight performance," *Astron. Astrophys.*, vol. 518, pp. 21–27, Jul. 2010.
[87] A. D. Turner *et al.*, "Silicon nitride micromesh bolometer array for submillimeter astrophysics," *Appl. Opt.*, vol. 40, pp. 4921–4932.
[88] R. J. Ivison, P. P. Papopoulos, I. Smail, T. R. Greve, A. P. Thomson, E. M. Xilouris, and S. C. Chapman, *Astron. Astrophys.*, vol. 518, pp. 190–193, 2010.
[89] I. Valtchanov *et al.*, "Physical conditions of the interstellar medium of high-redshift, strongly lensed submillimetre galaxies from the Herschel-ATLAS," *Monthly Notices Roy. Astronom. Soc.*, 2011.
[90] E. E. Becklin and R. D. Gehrz, "Stratospheric observatory for infrared astronomy (SOFIA)," in *SPIE Conf. Ser.*, Aug. 2009, vol. 7453, pp. 745302-745302-I2–745302-745302-I2.
[91] R. Klein *et al.*, "FIFI LS getting ready to fly aboard SOFIA," in *SPIE Conf. Ser.*, Jul. 2010, vol. 7735, pp. 77351T-77351T-8–77351T-77351T-8.
[92] R. Giovanelli *et al.*, CCAT, [Online]. Available: http://www.submm.org/sci/astro2010/Giovanelli-CCAT.pdf
[93] C. M. Bradford *et al.*, "Z-spec: A broadband millimeter-wave grating spectrometer: Design, construction, and first cryogenic measurements," in *SPIE Conf. Ser.*, Oct. 2010, vol. 5498, pp. 257–257.
[94] C. M. Bradford *et al.*, "The warm molecular gas around the Cloverleaf Quasar," *Astrophys. J.*, vol. 705, pp. 112–122, Nov. 2009.
[95] P. F. Goldsmith and M. Seiffert, "A flexible quasioptical input system for a submillimeter multiobject spectrometer," *Publications Astronom. Soc. Pacific*, vol. 121, pp. 735–742.
[96] T. Nakagawa, "The next-generation space infrared astronomy mission SPICA," in *SPIE Conf. Ser.*, Jul. 2010, vol. 7731, pp. 77310O-7–77310O-8.
[97] B. Swinyard *et al.*, "The european contribution to the SPICA mission," in *SPIE Conf. Ser.*, Aug. 2008, vol. 7010, pp. 70100I-7–770100I-8.
[98] J. R. Houck *et al.*, "The infrared spectrograph (IRS) on the spitzer space telescope," *Astrophys. J. Supplement Series*, vol. 154, pp. 18–24, Sep. 2004.
[99] C. M. Bradford *et al.*, "The background-limited infrared-submillimeter spectrograph (BLISS) for SPICA: A design study," in *SPIE Conf. Ser.*, Jul. 2010, vol. 7731, pp. 77310S1-12–77310S1-12.
[100] L. Ferrarese and D. Merrit, "A fundamental relation between supermassive black holes and their host galaxies," *Astrophys. J.*, vol. 539, pp. L9–L12, Aug. 2000.
[101] K. Gebhardt *et al.*, "A relationship between nuclear black hole mass and galaxy velocity dispersion," *Astrophys. J.*, vol. 539, pp. L13–L16, Aug. 2000.

Gordon J. Stacey was born in Chicago, IL, on August 25, 1957. He received the B.A. degree in physics and mathematics at Grinnell College, Grinnell, IA, in 1979, and the Ph.D. degree in astronomy from Cornell University, Ithaca, NY, in 1985.

He was first a Postdoctoral Associate, then a Research Physicist in the Physics Department at UC Berkeley from 1985 until 1991. In 1991 he obtained a faculty position in the Astronomy Department at Cornell University, where is now Professor of Astronomy.

Prof. Stacey is a member of the American Astronomical Society and the International Astronomical Union.